

Check for updates

APPROVED: 26 September 2024 doi: 10.2903/sp.efsa.2024.EN-9049

Elucidating the influence of wild boar density on African swine fever spread in wild boar populations, Italy, 2022–2023

B. H. Hayes¹, J. S. Lim^{1,2}, M. Andraud², T. Vergne¹

¹ IHAP, University of Toulouse, INRAE, ENVT, Toulouse, France

² Ploufragan-Plouzané-Niort Laboratory, ANSES, Ploufragan, France

Abstract

Wild boar density has been suggested to play a role in shaping African swine fever (ASF) transmission patterns. To provide quantitative estimates of the influence of wild boar density on ASF spread, a spatially-explicit detection-delay SIR mechanistic model of ASF transmission among density-explicit wild boar habitat was developed and parameterised to observed epidemic data in northern Italy from January 2022 through September 2023. Wild boar density estimates were generated by the ENETWILD consortium. Infectious periods, local prevalence at time of first detection, detection rates, and seasonal recovery rates were estimated directly from surveillance data. Eight models were constructed utilizing static and seasonal transmission rates along with linear relationships between habitat susceptibility/infectivity and wild boar density. Transmission rate, relative susceptibility, and relative infectivity were estimated by fitting each model to the observed epidemic using sequential Monte Carlo approximate Bayesian computation. The model that most closely fit the full data used a seasonal transmission rate but did not support a wild boar density effect on ASF spread across the entire study period. However, further analyses of the model outputs suggest that wild boar density likely played a role in shaping ASF transmission patterns during the second wave only (October 2022 - September 2023). This observation could be due to a lack of power in the first wave, lower surveillance rates in that period, or be from density estimates no longer reflecting the true wild boar density distributions upon the start of the second wave. These results demonstrate that wild boar density impacted ASF propagation in northern Italy. Further investigation by estimating parameters for individual epidemic waves could be beneficial to better characterise the wave-specific impact of wild boar density. The model developed here could be used in other contexts to evaluate if the influence of wild boar density is present across epidemic scenarios.

© European Food Safety Authority, 2024

Keywords: Simulation modelling, stochastic, SIR, wildlife, disease dynamics, infectious disease

Question number: EFSA-Q-2024-00530

Correspondence: biohaw@efsa.europa.eu



23978325, 2024, 11, Downloaded from https://efsa.onlinelibrary.wiley.com/doi/10.2903/sp.efsa.2024.EN-9049 by Istituto Zooprofilattico Sperimenta dell'Umbria e delle Marche (IZSUM), Wiley Online Library on [04/12/2024]. See the Terms and Conditions (https://onlinelibrary.

and-conditions) on Wiley Online Library for rules of use; OA articles are governed by the applicable Creative Commons

Disclaimer: The present document has been produced and adopted by the bodies identified above as author(s). This task has been carried out exclusively by the author(s) in the context of a contract between the European Food Safety Authority and the author(s), awarded following a tender procedure. The present document is published complying with the transparency principle to which the Authority is subject. It may not be considered as an output adopted by the Authority. The European Food Safety Authority reserves its rights, view and position as regards the issues addressed and the conclusions reached in the present document, without prejudice to the rights of the authors.

Acknowledgements: We thank Hans-Hermann Thulke for providing external review of the manuscript and contributing valuable insights.

Suggested citation: Hayes BH, Lim JS, Andraud M and Vergne T, 2024. Elucidating the influence of wild boar density on African swine fever spread in wild boar populations, Italy, 2022–2023. EFSA supporting publication 2024:EN-9049. 40 pp. doi:10.2903/sp.efsa.2024.EN-9049

ISSN: 2397-8325

© European Food Safety Authority, 2024

Reproduction is authorised provided the source is acknowledged.

EFSA may include images or other content for which it does not hold copyright. In such cases, EFSA indicates the copyright holder and users should seek permission to reproduce the content from the original source.

Map disclaimer: The designations employed and the presentation of material on any maps included in this scientific output do not imply the expression of any opinion whatsoever on the part of the European Food Safety Authority concerning the legal status of any country, territory, city or area or of its authorities, or concerning the delimitation of its frontiers or boundaries.







To provide quantitative estimates of the influence of wild boar density on African swine fever (ASF) spread, a spatially-explicit detection-delay SIR mechanistic model of ASF transmission among density-explicit wild boar habitat was developed and parameterised to observed epidemic data in northern Italy from January 2022 through September 2023.

Briefly, laboratory results from wild boar carcasses were collected by EFSA for Italy, containing the date of carcass detection, method of carcass detection, the ASF virus polymerase chain reaction (PCR) laboratory result (positive or negative) and the explicit coordinates of the carcass location. The study period was defined empirically as the day the first ASF-positive carcass was found (January 2022) through the end of the last complete epidemic wave (September 2023). The ENETWILD consortium provided wild boar abundance estimations as a discrete-space two-dimensional cell grid at 4 km² resolution, with each 2 km x 2 km cell containing the estimated number of individual wild boar per square kilometer. In the study area, estimated wild boar densities ranged from 2.5 to 9.4 individuals (mean 5.66) per square kilometer.

The model explicitly represented ASF transmission processes between 4-km² cells and accounted for imperfect detection due to heterogeneous surveillance efforts. The model did not explicitly represent within-cell infection dynamics. More specifically, each cell could cycle through four sequential states: susceptible (S), infectious-undetected (Iu), infectiousdetected (Id) and recovered, with the potential for returning to susceptibility following recovery. The transitions from one state to the next were governed by epidemiological parameters that were derived either empirically from the observed data (i.e. the rates of transition from Iu to Id, from Id to R or from R back to S) or by algorithmically calibrating the model to the observed epidemic (i.e. the transmission rate, which informs the force of infection). The force of infection, that governs the rate at which a susceptible cell becomes infected, was expressed as a function of the relative susceptibility of the susceptible cell, the relative infectivity of the infectious cells and the transmission rate. The relative susceptibility and infectivity of a cell could each be considered either dependent on the wild boar density of that cell (with a parameter defining this dependence to be estimated) or be equal to 1 (to mimic a situation where all cells would be equally susceptible or infective, irrespective of their wild boar density). The transmission rate was considered either constant (one parameter to be estimated) or seasonal (two parameters to be estimated). These different formulations for these three parameters defined eight different models, which were all calibrated to the Italian epidemic through an adaptive population Monte Carlo algorithm and compared to each other using the overall distance between the simulated and the observed summary statistics upon completion of the model calibration phase.

Having reproduced the two ASF waves observed during the study period, the best-fitting model used a seasonal transmission rate, indicating that the temporal variation in ASF transmission rates was informative in replicating the observed transmission patterns. It also did not account for wild boar density to adjust the susceptibility or the infectivity of the cells, suggesting that wild boar density did not play a constant role in better-informing ASF spread across the two epidemic waves.

www.efsa.europa.eu/publications





23978325, 2024, 11, Downloaded from https://efsa.onlineltbrary.wiley.com/doi/10.2903/sp.efsa.2024.EN-9049 by Istituto Zooprofilatico Sperimenta dell'Umbria e delle Marche (IZSUM), Wiley Online Library on 1041 20204]. See the Terms and Conditions (https://onlineltbrary.wiley.com/terms-and-conditions) on Wiley Online Library for rules of use; OA articles are governed by the applicable Creative Commons

To refine the assessment of the impact of wild boar density on ASF spread, we compared the proportion of higher density cells (those above the mean density) that had tested positive during the first or second wave to the distribution that would be expected under the model that did not account for a wild boar density effect (which happens to be the best-fitting model). We found that wild boar density was an influencing factor on ASF spread during the second wave, but not during the first.

The calibrated model was also used to estimate epidemic progression rates. In the first wave, the maximum rate of growth was seen in February (2022) with an average monthly median value of 44 km^2 per week (CI₉₅ 0, 132). In the second wave, the maximum rate of growth was seen in January (2023) with an average monthly median value of 124 km^2 per week (CI₉₅ 29, 268).

It is possible that the apparent lack of an influence of wild boar density in ASF spread during the first wave could be the result of a lack of power, since the first wave only lasted 38 weeks, as opposed to the full 52-week period seen in the second wave. Additionally, the surveillance outcomes were not equal between the two waves. During the first wave, 771 carcasses were located averaging 20.3 carcasses per week, while during the second wave 1503 carcasses were located averaging 28.9 carcasses per week, over approximately the same surface area. The lower surveillance rate seen during the first wave could also be a factor in the apparent lack of influence of density. Analysing the subsequent epidemic wave (September 2023 through October 2024) could be useful for refining this assessment. It must be kept in mind that the wild boar abundance estimates that were used as a model input refer to the period prior to ASF emergence. It is probable that the wild boar abundance distribution across the study period when the second wave started (September 2022) no longer reflected the assumed distribution, introducing a potential bias in the analysis.

In addition, this model could be explored further to investigate if wild boar density thresholds could be identified that would allow natural fade-outs of ASF spread (which previous investigation attempts had failed to identify). Finally, the model should now be validated against other contexts of ASF emergence (e.g. Belgium, Germany or Sweden), to evaluate if the influence of wild boar density is present across epidemic scenarios.





Table of Contents

Abstra	nct	1
Summ	nary	3
Table	of Contents	5
1	Introduction	6
1.1	Background and terms of reference as provided by the requestor	6
2	Data and methodologies	7
2.1	Overview	7
2.2	Data	7
2.3	Methodologies	8
2.3.1	Model parameterisation	8
2.3.2	Infection process simulation	10
2.3.3	Model calibration	11
2.3.4	Model selection	11
2.3.5	Model analysis	11
2.3.6	Spatial progression	12
3	Assessment/Results	12
3.1	Epidemiological overview	
3.2	Best-performing model	14
3.3	Parameter estimates	15
3.4	Simulated dynamics	17
3.5	Density assessment	19
3.6	Spatial progression	20
4	Discussion	
5	Conclusions and recommendations	23
Refere	ences	24
Abbre	viations	27
APPEN	IDIX A - ODD (Overview Design concepts Details)	28

rights of the authors.





ded from https://efs.aonlinelibary.wikey.com/doi/10.2993/sp.efsa.2024.EN-9049 by Istituto Zooprofilatico Sperimentad ell'Umbria e delle Marche (IZSUM), Wikey Online Library on [04/12/2024]. See the Terms and Conditions (https://omlehibrary.wiley.com/terms-and-conditions) on Wiley Online Library for rules of tase; Os Aarticles are governed by the applicable Cereive Commons



Introduction 1

In 2022 EFSA received a mandate from the European Commission to provide technical and scientific assistance on African swine fever (ASF) until 2028. In the context of Article 31 of Regulation (EC) No. 178/2002, EFSA should deliver every two years a Scientific Report analysing the risk factors involved in the occurrence, spread and maintenance of ASF virus, with a view to inform risk management and enable the preparation of future risk assessments.

Among those, the third element of the mandate requests to assess the risk factors, including wild boar density, on occurrence, spread and persistence of ASF in wild boar populations in Europe. Different methodologies can be used for this purpose. However, mechanistic models are considered the most suitable tool to simulate the spread of ASF in wild boar populations and to assess the impact of risk factors on the spread and maintenance of the disease.

This call is based on EFSA's 2023 Work Programme for grants and operational procurements as presented in Annex XII of the Programming Document 2023 - 2025, available on the EFSA's website¹.

1.1 Background and terms of reference as provided by the requestor

The contract entitled "Development of a mechanistic model to quantify the influence of wild boar density on African swine fever spread and maintenance in wild boar population" was awarded by EFSA to the Institut National de Recherche pour l'Agriculture, l' Alimentation et I' Environment (INRAE) (contract number NP/EFSA/BIOHAW/2024/01).

The objective of this contract was to provide quantitative estimates on how wild boar density influenced the transmission dynamics of ASF in a wild boar population, with a specific focus on the susceptibility (capacity to become infected) and transmissibility (capacity to infect) of wild boar habitats and on the persistence of the infection (duration of infectiousness) in wild boar habitats.

For that purpose, a spatially-explicit multi-host model of ASF transmission, previously developed for the transmission of ASFv in both domestic and wild boar populations (Hayes et al., 2024 under revision) will be adapted to represent the wild boar population in coherence with other tasks from the ASF working group (2x2 km cells) and to incorporate the new parameters of interest in order to simulate accurately the spread of ASFv in the selected wild boar populations. The model will then be parametrised to historical ASF epizootics of relevance (to be defined by the working group) using ASF surveillance data from the selected scenarios and the latest data available on wild boar density at the highest resolution. The relevant ASF surveillance data will be provided by the ASF working group and the relevant wild boar density data will be provided by the ENETWILD consortium.

¹ https://www.efsa.europa.eu/sites/default/files/2022-01/amp2325.pdf



EFSA Supporting publication 2024:EN-9049

www.efsa.europa.eu/publications

The present document has been produced and adopted by the bodies identified above as authors. This task has been carried out exclusively by the authors in the context of a contract between the European Food Safety Authority and the authors, awarded following a tender procedure. The present document is published complying with the transparency principle to which the Authority is subject. It may not be considered as an output adopted by the Authority. The European Food Safety Authority reserves its rights, view and position as regards the issues addressed and the conclusions reached in the present document, without prejudice to the rights of the authors.





aded from https://efsa.onlinelibrary.wiley.com/doi/10.2903/sp. efsa.2024.EN-9049 by Istituto Zooprofilattico Sperimenta dell'Umbria e delle Marche (IZSUM), Wiley Online Library on [04/12/2024]. See the Terms and Conditions (https://onlinelibrary.wiley.com/doi/10.2903/sp. efsa.2024.EN-9049 by Istituto Zooprofilattico Sperimenta dell'Umbria e delle Marche (IZSUM), Wiley Online Library on [04/12/2024]. See the Terms and Conditions (https://onlinelibrary.wiley.com/doi/10.2903/sp. efsa.2024.EN-9049 by Istituto Zooprofilattico Sperimenta dell'Umbria e delle Marche (IZSUM). Wiley Online Library on [04/12/2024]. See the Terms and Conditions (https://onlinelibrary.wiley.com/doi/10.2903/sp. efsa.2024.EN-9049 by Istituto Zooprofilattico Sperimenta dell'Umbria e delle Marche (IZSUM). Wiley Online Library on [04/12/2024]. See the Terms and Conditions (https://onlinelibrary.wiley.com/doi/10.2903/sp. efsa.2024.EN-9049 by Istituto Zooprofilattico Sperimenta dell'Umbria e delle Marche (IZSUM). Wiley Online Library on [04/12/2024]. See the Terms and Conditions (https://onlinelibrary.wiley.com/doi/10.2903/sp. efsa.2024.EN-9049 by Istituto Zooprofilattico Sperimenta dell'Umbria e delle Marche (IZSUM). Wiley Online Library on [04/12/2024]. See the Terms and Conditions (https://onlinelibrary.wiley.com/doi/10.2903/sp. efsa.2024.EN-9049 by Istituto Zooprofilattico Sperimenta dell'Umbria e delle Marche (IZSUM). Wiley Online Library on [04/12/2024]. See the Terms and Conditions (https://onlinelibrary.wiley.com/doi/10.2903/sp. efsa.2024.EN-9049 by Istituto Zooprofilattico Sperimenta dell'Umbria e delle Marche (IZSUM). Wiley Online Library on [04/12/2024]. See the Terms and Conditions (https://onlinelibrary.wiley.com/doi/10.2903/sp. efsa.2024.EN-9049 by Istituto Zooprofilattico Sperimenta dell'Umbria e de



The results of the best-fitted model would serve to estimate the contribution of the different parameters, with special emphasis on wild boar density, to ASF infection dynamics in wild boar in selected locations.

2 Data and methodologies

2.1 Overview

A complete and detailed model description, following the ODD (Overview, Design concepts, Details) protocol (Grimm et al., 2006) is provided as Appendix A . All scripts used to perform this research are publicly available through Zenodo (Hayes et al., 2024). The basic premise underlying the ASF wild boar density assessment model was that ASF spread among wild boar will be seen to spread near-contiguously through interconnected wild boar habitat in a highly surveyed environment. This pattern of spread could be modulated by local wild boar densities, which were investigated through an agent-based transmission model using density-explicit 2 km x 2 km wild boar habitat cells as entities. The ASF infection process occurred via a detection-delay SIRS mechanistic epidemiological model. By calibrating transmission parameters to the observed epidemic, and informing other infection state processes (i.e. rates of detection, recovery, return to susceptibility) from the observed data, the observed dynamics could be simulated. The overall purpose of the model was to inform the impact of wild boar density in explaining observed ASF transmission patterns among wild boar.

Italy was chosen to host the final location of study. Here, the available national surveillance data included both positive and negative laboratory results that were tied to explicit coordinate locations for each carcass, and being an emerging situation, the state of the population at the start of the modelled period was known. Further, wild boar density estimates in the region were among the most-accurate in Europe, being informed by both habitat suitability and hunting yield estimates, later calibrated with information from local camera traps.

2.2 Data

The ASF wild boar density assessment model was constructed from spatially-explicit ASF surveillance data and gridded wild boar density estimate data. National ASF surveillance data in Italy for wild boar carcasses, provided by the European Food Safety Authority (EFSA) for the period January 2022 - December 2023, contained information on the date of carcass detection, the method of detection (found dead, hunted, or road/predator killed), the ASF virus polymerase chain reaction (PCR) laboratory result for the tested carcass (positive or negative), and the explicit coordinates of the carcass location. ASF clusters were identified through nearest-neighbourhood contiguity of found-dead wild boar carcasses, assuming a maximum transmission distance of 20 km between related cases. A minimum convex polygon around the largest case cluster, plus a 20 km buffer, was used to define the region of study. The study period was defined as the period between the onset of the epidemic and the end of the last complete epidemic wave (September 2023). Surveillance data was binned per 2

EFSA Supporting publication 2024:EN-9049

www.efsa.europa.eu/publications





3.978325, 2024.11, Downwaled from https:///sta.onlinelbury.wikey.com/doi/10.29036, peksa.2024.EN-9049 by Istituto Zooprofilatics Sperimenta dell'Umbria e delle Marche (IZSUM), Wiley Online Library on [04/12/2024]. See the Terms and Conditions (https://onlinelbury.wikey.com/doi/10.29036, peksa.2024.EN-9049 by Istituto Zooprofilatics Sperimenta dell'Umbria e delle Marche (IZSUM), Wiley Online Library on [04/12/2024]. See the Terms and Conditions (https://onlinelbury.wikey.com/doi/10.29036, peksa.2024.EN-9049 by Istituto Zooprofilatics Sperimenta dell'Umbria e delle Marche (IZSUM), Wiley Online Library on [04/12/2024]. See the Terms and Conditions (https://onlinelbury.wikey.com/doi/10.29036, peksa.2024.EN-9049 by Istituto Zooprofilatics Sperimenta dell'Umbria e delle Marche (IZSUM), Wiley Online Library on [04/12/2024]. See the Terms and Conditions (https://onlinelbury.wikey.com/doi/10.29036, peksa.2024.EN-9049 by Istituto Zooprofilatics Sperimenta dell'Umbria e delle Marche (IZSUM), Wiley Online Library on [04/12/2024]. See the Terms and Conditions (https://onlinelbury.wikey.com/doi/10.29036, peksa.2024.EN-9049 by Istituto Zooprofilatics Sperimenta dell'Umbria e delle Marche (IZSUM), Wiley Online Library on [04/12/2024]. See the Terms and Conditions (https://onlinelbury.wikey.com/doi/10.29036, peksa.2024.EN-9049 by Istituto Zooprofilatics (https://onlinelbury.wikey.com/doi/10.29036, peksa



km x 2 km cell, and infectious period durations at the cell level were calculated for each cell (see Appendix A §A.3.4.1.1(iii) for details).

The ENETWILD consortium previously estimated wild boar distribution and abundance throughout Europe as a discrete-space two-dimensional cell grid at 4 km² resolution, with each 2 km x 2 km cell containing the estimated number of individual boar per square kilometer (ENETWILD consortium, 2024). The cells located within the study region were extracted to comprise the local wild boar density habitat grid.

2.3 Methodologies

2.3.1 Model parameterisation

Parameters that inform model processes are listed in **Table 1**. Regarding parameters informed directly from the surveillance data, infectious periods per cell were calculated as the sum of overlapping individual infectious periods for each detected carcass within that cell, assuming a 4-week delay between infection and detection, and either a 2- or 4-week period of persisting environmental infectiousness after carcass detection (and removal) in the nonwinter (mid-February through the end of November) or winter (December through mid-February) periods, respectively. The detection delay itself is the sum of the time from infection until death and death until carcass detection. The former is estimated at two weeks (Guinat et al., 2018). Estimated delay in carcass detection was informed from expert opinion on levels of carcass decomposition upon discovery in a highly-surveyed setting (South Korea), and is also approximately two weeks (J.-S. Lim, personal communication, May 2024). Together this yields an estimated detection delay of four weeks per carcass. (see §A.3.4.1.1(iii). for details). Detection rates were calculated per cell per week based on the estimated prevalence of ASF upon first detection and the surveillance effort, defined as the number of carcasses found and tested in that cell at week t (§A.3.4.1.1(iv)). Mean seasonal recovery rates were informed from cell infectious periods (§A.3.4.1.1(v)). Distinct epidemic waves were observed in the weekly cell-level incidence, and were used to inform the weeks at which cells in the recovered state could transition back to the susceptible state. The initial infectious cells were defined from the surveillance data as any cell in the first ISO week of the surveillance data in which a case was detected.

Parameters not informed directly by the data—transmission rate (either static or seasonal following a sinusoidal function with a one-year period), relative infectivity and relative susceptibility of cells with the lowest wild boar density as compared to the cells with the highest wild boar density—were estimated numerically during model calibration.









Name	Description	Value ^(a)	Course
Name	Description		Source
Transmission rate $(\beta \text{ or } \beta_t)$	Static (β) or seasonal (β_t) cell-to-cell transmission rate	Estimated during model fitting process	APMC calibration ²
Amplitude (A)	Maximum annual transmission rate in sinusoidal function	Estimated during model fitting process	APMC calibration
Phase shift (u)	Sinusoidal function relative shift from 0°	Estimated during model fitting process	APMC calibration
Detection rate $(\varepsilon_{i,t})$	Detection rate of infected cell i during week t	$-\ln(1-P_{i,t})$	Observed data
Probability of detection $(P_{i,t})$	Probability of detection of at least one positive carcass in cell <i>i</i> during week <i>t</i>	$1-(1-\pi_{det})^{n_{i,t}}$	Observed data
Number of carcasses tested $(n_{i,t})$	Number of carcasses tested in cell <i>i</i> during week <i>t</i>	Variable by weekly incell surveillance effort	Observed data
ASF prevalence at first detection (π_{det})	Proportion of positive carcasses in infected cells at first detection	0.89	Observed data
Recovery rate (γ_t)	Mean seasonal recovery rate of cells during week t	0.14 cells/week (non- winter) 0.095 cells/week (winter)	Observed data
Resusceptibility transition (σ)	Week of calendar year for recovered cells to transition back to susceptible state	Week 38	Observed data
Relative susceptibility (φ)	Relative susceptibility of lowest density cells	Estimated during model fitting process	APMC calibration
Relative infectivity (ψ) ASF individual	Relative infectivity of lowest density cells Average infectious period	Estimated during model fitting process 2 weeks	APMC calibration
infectious period	duration of individual wild boar		
ASF environmental infectious period	Average seasonal duration of environmental infectiousness persistence	4 weeks (non-winter) 6 weeks (winter)	(Guberti et al., 2022)
Carcass detection delay	Average delay from death to carcass detection	2 weeks	(JS. Lim, personal communication, May 2024)
Winter period	Continuous yearly period with median temperature < 5°C	First week of December through second week of February	(Agenzia regionale per la protezione ambientale (ARPA) Liguria, Lombardia, & Piemonte, 2024)
Non-winter period	Yearly period outside of winter period	Third week of February through last week of November	(Agenzia regionale per la protezione ambientale (ARPA) Liguria, Lombardia, & Piemonte, 2024)

² Adaptive population Monte Carlo (APMC), a variant of the sequential Monte Carlo algorithm in approximate Bayesian computation (ABC-SMC) (Lenormand et al., 2012)

www.efsa.europa.eu/publications



EFSA Supporting publication 2024:EN-9049

The present document has been produced and adopted by the bodies identified above as authors. This task has been carried out exclusively by the authors in the context of a contract between the European Food Safety Authority and the authors, awarded following a tender procedure. The present document is published complying with the transparency principle to which the Authority is subject. It may not be considered as an output adopted by the Authority. The European Food Safety Authority reserves its rights, view and position as regards the issues addressed and the conclusions reached in the present document, without prejudice to the rights of the authors.





ded from https://efsa.onlinelibrary.wiley.com/doi/10.2903/sp.efsa.2024.EN-9049 by Istituto Zooprofilattico Sperimenta dell'Umbria e delle Marche (IZSUM), Wiley Online Library on [04/12/204]. See the Terms and Conditions (https://onlinelibrary.wiley.com/terms-

and-conditions) on Wiley Online Library for rules of use; OA articles are governed by the applicable Creative Commons



Infection states followed a detection-delay SIRS mechanistic epidemiological model, with individual cells cycling through four possible states of infection: susceptible (S), infectiousundetected (I_u) , infectious-detected (I_d) , and recovered (R), with the potential for returning to the susceptible state following recovery (Figure 1). Latency was not considered as the model operated on a geographic (as opposed to individual) scale with minimum cell infectious periods of four weeks; the 2-4 day latent period of ASF seen in wild boar (Blome et al., 2013; Pietschmann et al., 2015) was considered to have a negligible contribution to overall dynamics.

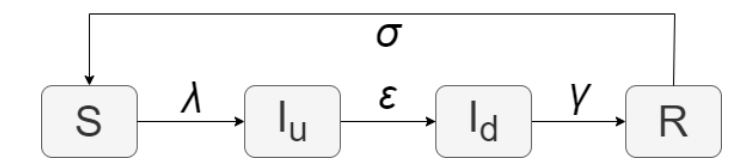


Figure 1. SIR infection state flow diagram. Model entities (cells) cycle through four possible states of infection: susceptible (S), infectious-undetected (I_u), infectious-detected (I_d), and recovered (R). Transitions to infectious and recovered states occur stochastically and are governed by the force of infection (λ) , detection rate (ε) , and recovery rate (γ) . Transition back to the susceptible state occurs deterministically and is specified by the calendar week of the year (σ) .

ASF transmission was simulated through a force of infection (λ) on susceptible cells that followed a frequency-dependent construction and was calculated for all susceptible cells experiencing non-zero infection pressure from all infected cells within the Moore neighbourhood (the first-order adjacent cells) of cell j, per Equation 1

$$\lambda_j = \varphi_j \sum_{t \in I_j} \psi_i * \beta_t / N_i \tag{1}$$

where λ_i is the force of infection exerted on susceptible cell j, φ_i is the relative susceptibility of cell j, ψ_i is the relative infectivity of infectious cell i, β_t is the transmission rate (at week tif seasonal), N_i is the number of cells in the Moore neighbourhood of cell i, and I_i is the set of all infectious cells neighbouring j.

The relative susceptibility of a cell was calculated as a function of its normalized density per Equation 2

$$\varphi_j = \rho_j + \varphi(1 - \rho_j) \tag{2}$$

where φ_i is the relative susceptibility of cell j, ρ_i is the normalized density of cell j, and φ is the estimated relative susceptibility for the lowest-density cells. Similarly, the relative infectivity of a cell was calculated as a function of its normalized density per Equation 3

www.efsa.europa.eu/publications







3978323, 2024, 11, Down loaded from https://efsa.on linelibrary.wiley.com/doi/10.2903/sp.efsa.2024.EN-9049 by Istituto Zogorofilattico Sperimenta dell'Umbria e delle Marche (IZSUM), Wiley Online Library on [04.12.2024]. See the Terms and Conditions (thtps://onlinelibrary.wiley.com/doi/10.2903/sp.efsa.2024.EN-9049 by Istituto Zogorofilattico Sperimenta dell'Umbria e delle Marche (IZSUM). Wiley Online Library on [04.12.2024]. See the Terms and Conditions (thtps://onlinelibrary.wiley.com/doi/10.2903/sp.efsa.2024.EN-9049 by Istituto Zogorofilattico Sperimenta dell'Umbria e delle Marche (IZSUM). Wiley Online Library on [04.12.2024]. See the Terms and Conditions (thtps://onlinelibrary.wiley.com/doi/10.2903/sp.efsa.2024.EN-9049 by Istituto Zogorofilattico Sperimenta dell'Umbria e delle Marche (IZSUM). Wiley Online Library on [04.12.2024]. See the Terms and Conditions (thtps://onlinelibrary.wiley.com/doi/10.2903/sp.efsa.2024.EN-9049 by Istituto Zogorofilattico Sperimenta dell'Umbria e delle Marche (IZSUM). Wiley Conditions (thtps://onlinelibrary.wiley.com/doi/10.2903/sp.efsa.2024.EN-9049 by Istituto Zogorofilattico Sperimenta dell'Umbria e delle Marche (IZSUM). Wiley Conditions (thtps://onlinelibrary.wiley.com/doi/10.2903/sp.efsa.2024.EN-9049 by Istituto Zogorofilattico Sperimenta dell'Umbria e delle Marche (IZSUM). Wiley Conditions (thtps://onlinelibrary.wiley.com/doi/10.2903/sp.efsa.2024.EN-9049 by Istituto Zogorofilattico Sperimenta dell'Umbria e delle Marche (IZSUM). Wiley Conditions (thttps://onlinelibrary.wiley.com/doi/10.2903/sp.efsa.2024.EN-9049 by Istituto Zogorofilattico Sperimenta dell'Umbria e delle Marche (IZSUM). Wiley Conditions (thttps://onlinelibrary.wiley.com/doi/10.2903/sp.efsa.2024.EN-9049 by Istituto Zogorofilattico Sperimenta dell'Umbria e delle Marche (IZSUM). Wiley Conditions (thttps://onlinelibrary.wiley.com/doi/10.2903/sp.efsa.2024.EN-9049 by Istituto Zogorofilattico Sperimenta dell'Endot (IZSUM). Wiley Conditions (thttps://onlinelibrary.wiley.com/doi/10.2903/sp.efsa.2024.EN-9049 by Istituto Z



 $\psi_i = \rho_i + \psi(1 - \rho_i)$ (3)

where ψ_i is the relative infectivity of cell i, ρ_i is the normalized density of cell i, and ψ is the estimated relative infectivity for the lowest-density cells. Transitions between the susceptible, infectious-undetected, infectious-detected, and recovered states occurred stochastically. The process for cells in the recovered state to return to the susceptible state was modelled deterministically and aligned to the weeks in which the observed epidemic waves ended.

Model calibration 2.3.3

Model calibration was performed through adaptive population Monte Carlo (APMC), a variation of sequential Monte Carlo approximate Bayesian computation (ABC-SMC) (Lenormand et al., 2012). Detailed explanation of the APMC process can be found in the ODD (Appendix A §A.3.4.1.4(vi)). The summary statistics that were used for model calibration reflected temporal and spatial dynamics as well as the wild boar density for 8 distinct periods in the 93 weeks over which the study occurred: for each period, we computed the number of cells detected (incidence), the surface area of the minimum convex polygon encapsulating all detected cells, and the sum of the wild boar density in detected cells. From these three metrics across eight aggregated periods, a total of 24 summary statistics were used to inform calibration.

2.3.4 Model selection

To assess the overall impact of density, eight models reflecting all transmission parameter combinations were fitted to the observed data. These models included those with either a static or seasonal transmission rate, with or without an effect of relative susceptibility modulated by wild boar density, and with or without an effect of relative infectivity modulated by wild boar density. The best-performing model was defined as the one with the closest distance to the summary statistics of the observed data upon completion of the model calibration phase.

2.3.5 Model analysis

The best-performing model was used to examine model outcomes from the conserved parameter estimates, including the apparent simulated incidence, the true simulated incidence, the detection probabilities per cell, and the prediction ability through a receiver operating characteristic (ROC) curve. Density was concluded as playing an influential role in explaining the observed epidemic dynamics over the entire study period if the best-performing model included at least one parameter informed by wild boar density (i.e. relative susceptibility, relative infectivity, or both). To explore if the impact of wild boar density was specific to individual epidemic waves, we used the null model—the model that was parameterised by only a transmission rate without any influence of wild boar density—that shared the same transmission rate function as the best performing model, and recorded the number of detected infected cells of high density (those above the median density of the study area) for both the observed data and for each simulation iteration. Within each epidemic wave, we counted the proportion of simulations for which the proportion of detected infected

www.efsa.europa.eu/publications







3978325, 2024, 11, Downloaded from https://efsa.onlinelibrary.wiley.com/doi/10.2903/sp.efsa.2024.EN-9049 by Istituto Zooprofilattico Sperimenta dell'Umbria e delle Marche (IZSUM), Wiley Online Library on [04/12/2024]. See the Terms and Conditions (https://onlinelibrary.wiley.com/derms-

and-conditions) on Wiley Online Library for rules of use; OA articles are governed by the applicable Creative Commons



cells of high wild boar density was greater that what was observed. If that proportion was lower than 5% we concluded that the apparent proportion of infected high-density cells in the observed data was higher than what would be observed according to a model that did not account for a wild boar density-dependent transmission process and therefore concluded that the wild boar density played a statistically significant role on that specific ASF epidemic wave.

2.3.6 Spatial progression

Using the true weekly infection status of cells in the best-fitting model, the weekly rate of epidemic progression per week was estimated. For each simulation, the cells contained within a minimum convex polygon encapsulating all infected cells up to a given week were used to define the spatial extent of the epidemic at that time. The difference in area between consecutive weeks was used to define the weekly rate of progression.

3 Assessment/Results

Epidemiological overview 3.1

The final study area consisted of 1,784 cells over an area of 7,136 km², intersecting the northern Italy regions of Liguria, Lombardy, and Piedmont (Figure 2). Estimated wild boar densities in the study area ranged from 2.5 to 9.4 wild boar/km², with a median of 5.7 wild boar/km². Across an 89-week period from 03 January 2022 through 16 September 2023, 2,274 wild boar carcasses were found dead with 751 (33%) carcasses testing positive for ASF. Surveillance effort varied weekly and by year, with an increase in the surveillance effort seen in 2023 compared to 2022 (Figure 3). When binned to the wild boar density grid, carcasses were detected and tested in 655 distinct cells. Of the tested cells, 278 contained at least one carcass that was ASF-positive, with a median of 2 cases per cell (Interquartile range [IQR] 1, 3; maximum 22).





Downloaded from https://els.ao.nlinelibrary.wiley.com/doi/10.2903/sp.efs.a.2024.EN-90.49 by Istituto Zooprofilatrico Sperimenta dell'Umbria e delle Marche (IZSUM), Wiley Online Library on [04/12/2024]. See the Terms and Conditions (https://oinlinelibrary.wiley.com/terms-ad-conditions) on Wiley Online Library for rules of uses (3.0 a trickes are governed by the applicable Certaine Commons



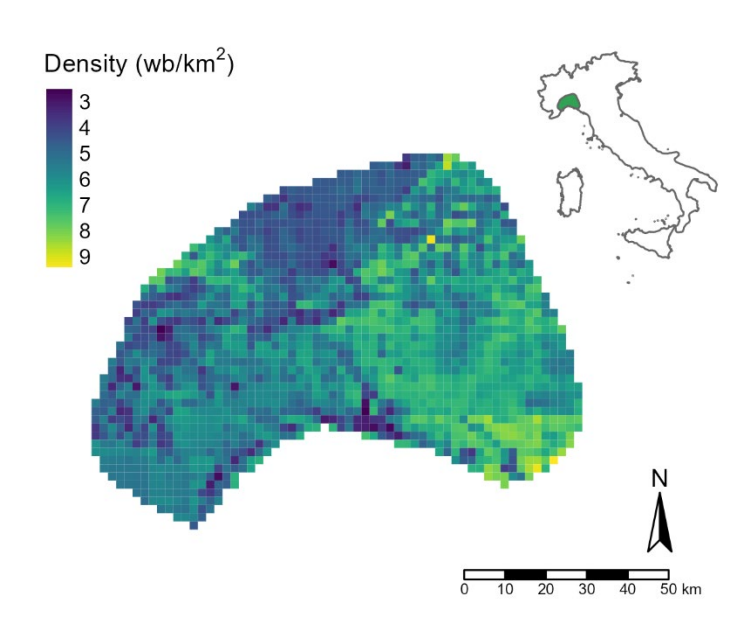


Figure 2. Gridded wild boar density estimates provided by the ENETWILD consortium in the final region of study, at 2 km x 2 km resolution (ENETWILD consortium, 2024). Estimated densities ranged from 2.9 to 9.4 (mean 5.7) individual wild boar per km2 (wb/km2). The study area corresponds to the green area shown in the national map inset for Italy.

The median estimated infectious period duration of a cell was 7.9 weeks (minimum 6 weeks, maximum 25 weeks). Reinfection events were defined as subsequent infectious periods within a cell where the estimated date of initial infection for the subsequent infectious period did not overlap with the estimated 4- or 6-week environmental infectious persistence period of the previous infectious period. It occurred a total of 85 times in 71 (4%) cells. Half of the reinfections (n = 36) occurred across the two epidemic waves. Of the reinfection events occurring within the same wave as the previous infection, 6 occurred in the first wave and 29 were observed in the second wave. The median weekly distance between the end of an initial cell infectious period and the subsequent infection was 2 weeks (IQR: 1, 5) in the first wave and 5 weeks (IQR: 2, 9) in the second. The mean ASF prevalence in carcasses around first detection n_{det} was computed at 0.89 (see §A.3.4.1.1(iv)). Detection rates ranged from 2.2 to 35 (IQR: 2.2, 2.2) cells per week, depending on the number of carcasses tested per cell per week (see Table 1 for equations). Mean seasonal recovery rates of cells were calculated at 0.14 cells/week in the non-winter period and 0.095 cells/week in the winter period (definitions provided in Table 1).



Jul - Dec 2023



ded from https://efsa.onlinelibrary.wiley.com/doi/10.2903/sp.efsa.2024.EN-9049 by Istituto Zooprofilattico Sperimenta dell'Umbria e delle Marche (IZSUM). Wiley Online Library on [04/12/2024]. See the Terms and Conditions (https://onlinelibrary.wiley.com/terms

and-conditions) on Wiley Online Library for rules of use; OA articles are governed by the applicable Creative Commons

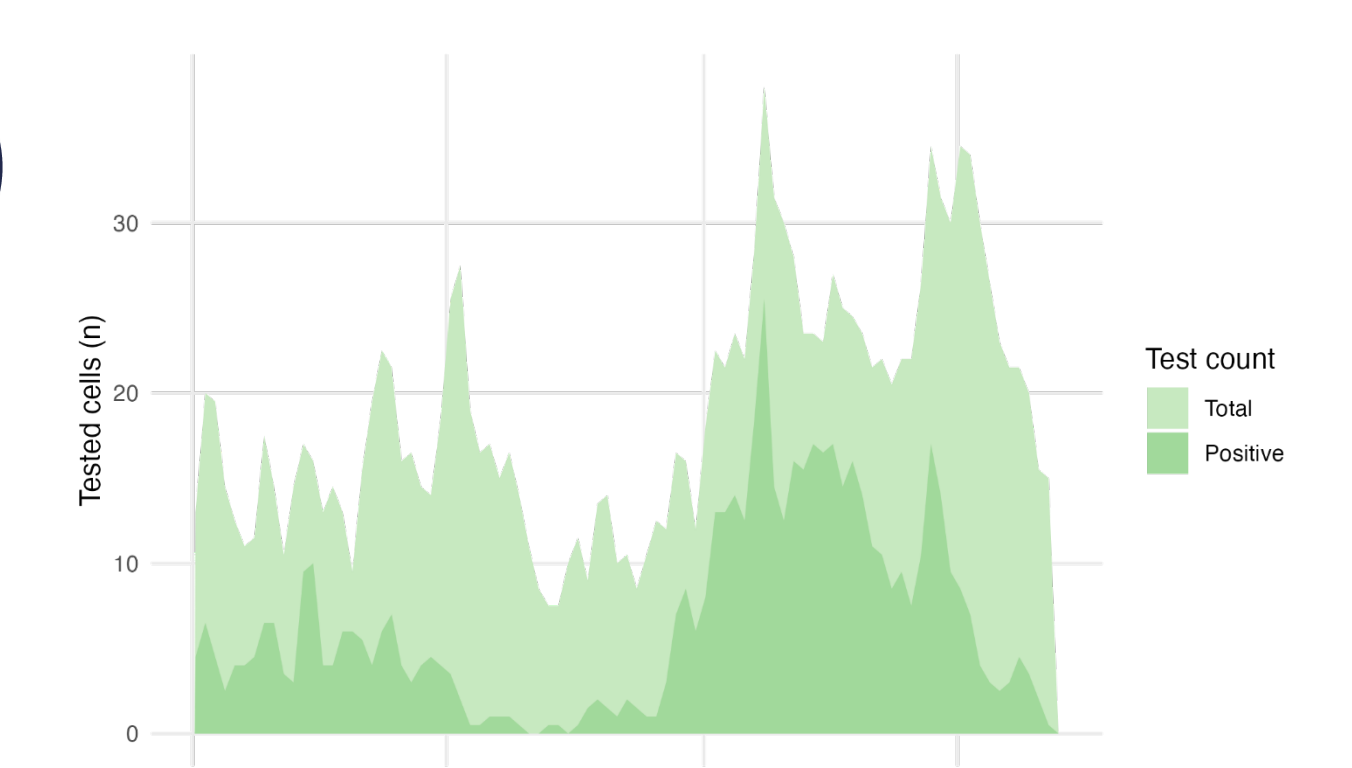


Figure 3. Surveillance effort showing total number of tested cells and number of tested cells with a positive carcass per week from January 2022 through September 2023.

Jan - Jun 2023

Jul - Dec 2022

3.2 Best-performing model

Jan - Jun 2022

All models that utilised a sinusoidal function for the transmission rate were observed to fit the observed carcass surveillance data better than the models which contained a constant transmission rate parameter (Figure 4), indicating that the temporal variation in ASF transmission rates played a substantial role in replicating observed detection patterns among cells. Further, models that utilized only a transmission rate function outperformed those models which had the same transmission rate function but accounted for relative susceptibility and/or a relative infectivity of cells as a function of wild boar density. This suggests that the transmission pattern was not driven by a wild boar density effect on cell susceptibility and infectivity across the study period within the study area. The model defined by only a sinusoidal transmission rate was considered as the best-fitting model and used for further interpretations.





37832, 2024. 1.1 Downkoaded from https://e8a.onlinelbrary.wisel.com/doi/10.2903/sp. efsa.2024.EN-9049 by Istituto Zoprofilatico Sperimenta dell'Umbria e delle Marche (IZSUM), Wely Online Library on [04/12/2024]. See the Terms and Conditions (https://onlinelbrary.wise). condend from the https://onlinelbrary.wise).



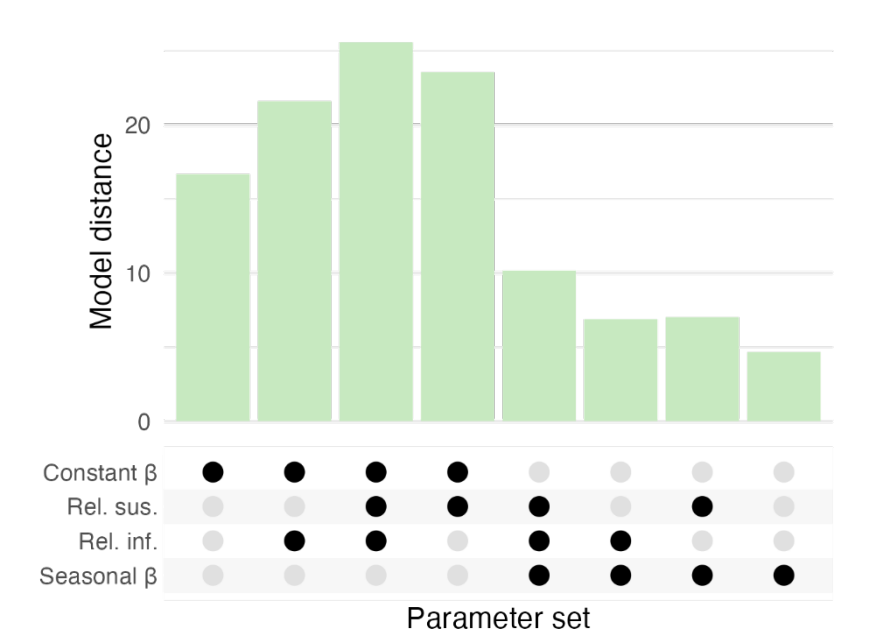


Figure 4. Upset plot of model distance between observed and simulated summary statistics by included parameters. Each model, defined through its combination of transmission parameters among a constant or seasonal transmission rate (β), cell relative susceptibility (rel. sus.), and cell relative infectivity (rel. inf.), is present along the x-axis. The parameters that define a model are visualized by the black dots in the matrix below the bar plot (e.g. the left-most model only includes a constant transmission rate parameter, while the second from left includes both constant transmission rate and relative infectivity parameters. The bestfitting model was defined as the one with the lowest distance from the observed data. Explicit distances are found in the supplemental material.

3.3 Parameter estimates

The amplitude (A) of the seasonal transmission rate was estimated at 0.27 (95% Credible interval $[CI_{95}]$ 0.23, 0.33), and its phase shift (ν) at 0.38 (CI_{95} 0.19, 0.56), from prior distributions $A \sim Uniform(0, 2)$ and $u \sim Uniform(0, 2)$ (**Figure 5**). From here, the seasonal transmission rate function that captured the observed transmission patterns could be reconstructed, and maximum and minimum transmission rate credible intervals were estimated (Figure 6). During the month of minimum transmission (July) the average weekly median transmission rate was 0.009 cells per week (CI₉₅ 0, 0.095), while during maximum transmission (January) the average weekly median transmission rate was 0.53 cells per week (CI₉₅ 0.44, 0.62).





37852, 2024, 1, 1, Dowlonded from https://efas.onlinelbary.wisley.com/doi/10.2993/sp.fe.a.com/con/in/com/by by Istituto Zooprofialatics Sperimena dell'Umbria e delle Marche (CZSUM), Wiley Online Library on [04/12/2024]. See the Terms and Conditions (https://onlinelbbrary.wisley.com/terms-and-conditions) on Wiley Online Library for rules of use; OA articles are governed by the applicable Creative Commons.



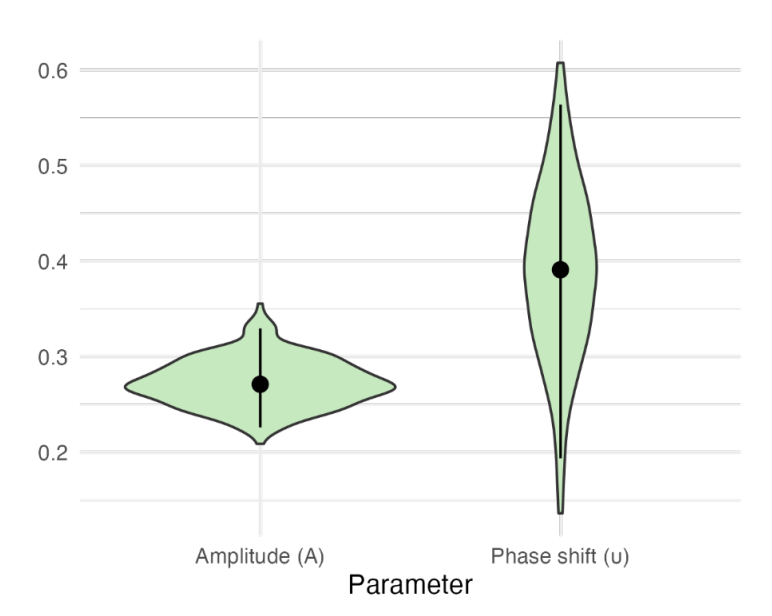


Figure 5. Posterior parameter estimates for the best-fitting model. The dot represents the median value of each parameter, while range bars indicate 95% credible intervals (CI95). Amplitude of the seasonal transmission rate was estimated at 0.27 (CI95 0.23, 0.33), and its phase shift at 0.39 (CI₉₅ 0.194, 0.56).

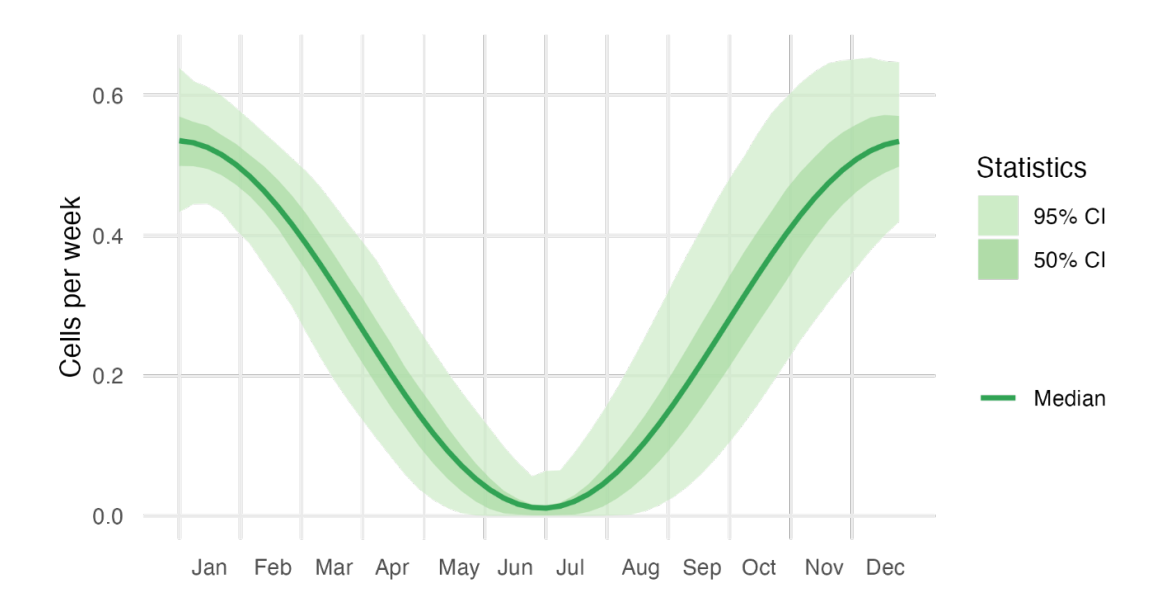


Figure 6. Seasonal transmission rate (β_t) as reconstructed from estimated amplitude (A) and phase shift (u) parameters. Light green and dark green ribbons reflect 95% and 50% credible intervals of the estimated transmission rates, respectively, with the median transmission rate given by the solid darkest green line. During the month of minimum transmission (July) the average weekly median transmission rate was 0.009 cells per week (CI95 0, 0.095), while during maximum transmission (January) the average weekly median transmission rate was 0.53 cells per week (CI₉₅ 0.44, 0.62).

www.efsa.europa.eu/publications



EFSA Supporting publication 2024:EN-9049

The present document has been produced and adopted by the bodies identified above as authors. This task has been carried out exclusively by the authors in the context of a contract between the European Food Safety Authority and the authors, awarded following a tender procedure. The present document is published complying with the transparency principle to which the Authority is subject. It may not be considered as an output adopted by the Authority. The European Food Safety Authority reserves its rights, view and position as regards the issues addressed and the conclusions reached in the present document, without prejudice to the rights of the authors.





ded from https://efsa.on/inelibrary.wiley.com/doi/10.2903/sp.efsa.2024.EN-9049 by Istituto Zooprofilattico Sperimenta dell'Umbria e delle Marche (IZSUM), Wiley Online Library on [04/12/2024]. See the Terms and Conditions (https://onlinelibrary.

and-conditions) on Wiley Online Library for rules of use; OA articles are governed by the applicable Creative Commons



Simulated dynamics 3.4

The model succeeded in replicating trends in observed incidence (Figure 7). A median difference of 4 infectious cells (maximum 15) per week in the first wave, and 12 infectious cells (maximum 27) in the second wave, was seen between the true and observed simulated data.

When examined spatially, trends in probabilities of detection of infectious cells were found to be congruent with spatial detection trends in the observed data, both overall and per-wave (Figure 8). Consistent with this visual spatial assessment, distinct differences in the expected probability of detection were seen between those cells that were detected as ASFV-positive in the observed data and those that were not (Figure 9). Cells without detected cases in the observed data had an expected probability of detection of 0.23 (IQR 0.04, 0.73) in the simulations, while cells containing detected cases in the observed data had an expected probability of detection of 0.83 (IQR 0.55, 0.95) in the simulations. A receiver operating characteristic (ROC) curve yielded an AUC of 0.78, indicating a moderate ability of the model to correctly discriminate between detected and non-detected cells in the observed data (Figure 9).

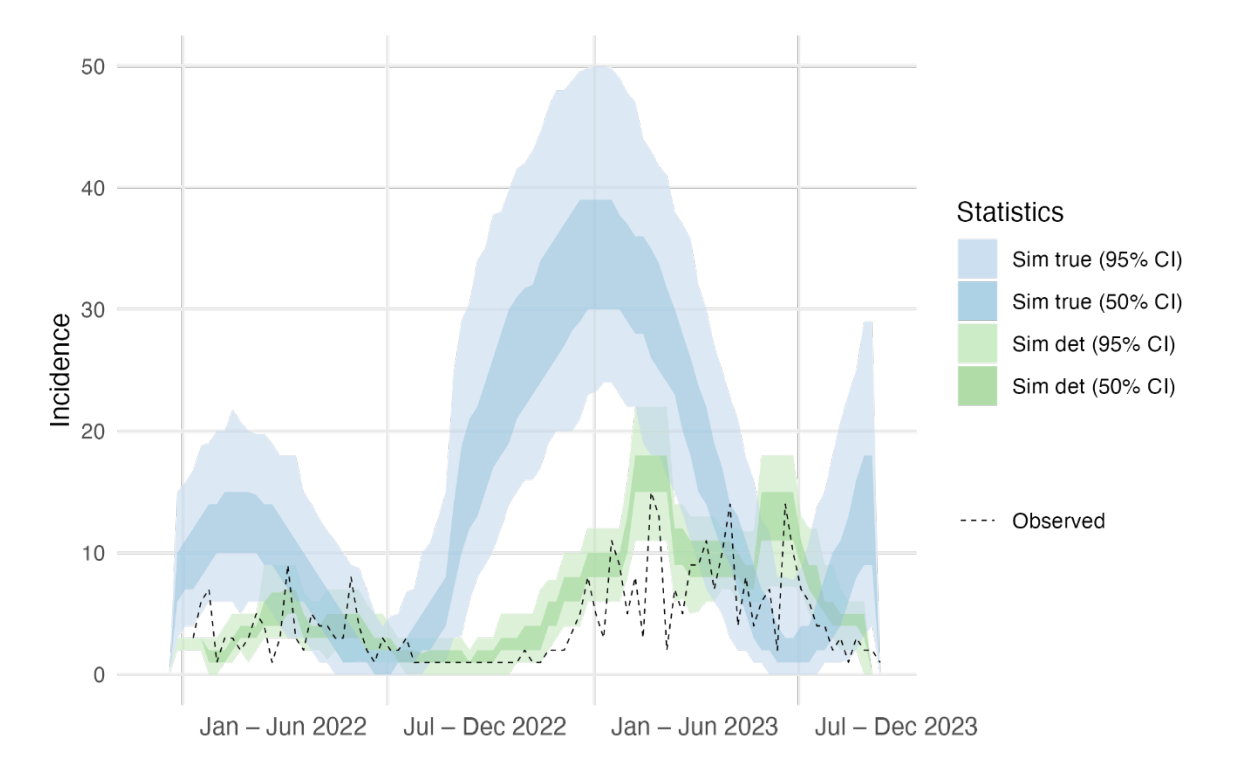


Figure 7. Simulated and observed weekly incidence at cell level. Simulated incidence is shown for both true simulated incidence in blue (derived from all infected cells) and apparent simulated incidence in green (derived from all infected cells that then were detected). The dotted line shows the apparent incidence in the observed data.

www.efsa.europa.eu/publications





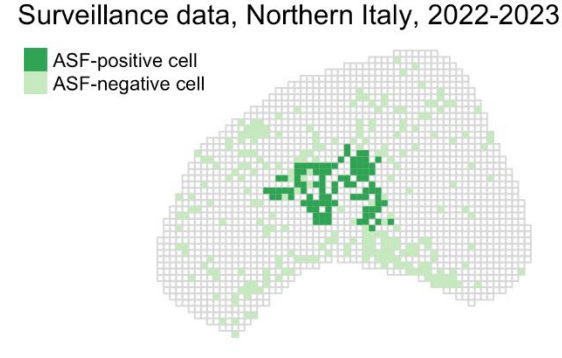


3978325, 2024, 11, Downloaded from https://efsa.onlinelibrary.wiley.com/doi/10.2903/sp.efsa.2024.EN-9049 by Istituto Zooprofilatico Sperimenta dell'Umbria e delle Marche (IZSUM), Wiley Online Library on 0/4/12/2024. See the Terms

and Conditions (https://onlinelibrary.wiley.com/terms-and-conditions) on Wiley Online Library for rules of use; OA articles are governed by the applicable Creative Commons

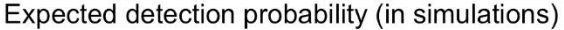


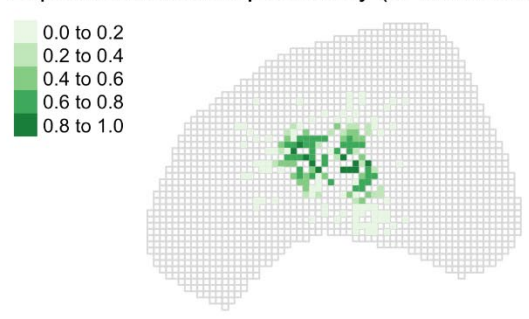
Wave 1

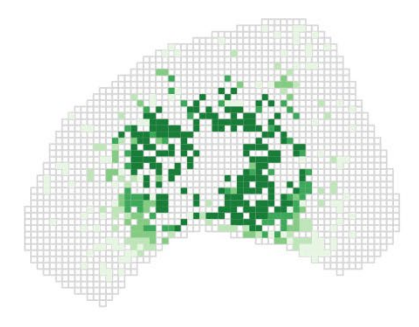


Wave 2









Expected infection probability

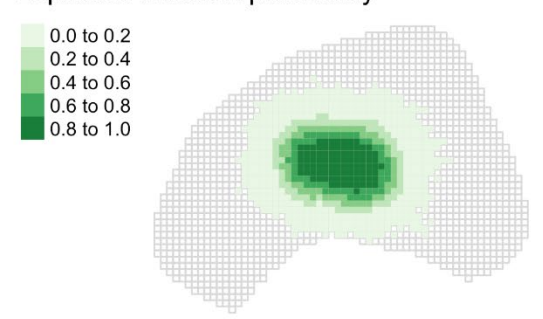




Figure 8. Maps of study area showing: the observed distribution of cells with detected cases (top); the expected detection probability for infectious cells, defined as the proportion of best-fitting model simulations in which the cells were detected as infected (middle); and the expected infection probability, defined as the proportion of best-fitting model simulations in which the cells were infected (bottom), partitioned by epidemic wave. Note that the detection probability of a cell integrates both the infection probability of that cell, as simulated by the model, and the number of carcasses tested in that cell, as informed by the surveillance data. Each cell represents a 2 km x 2 km area.







397832,5. 2024, 11, Downloaded from https://efsa.onlinelibrary.wiley.com/drio/10.2903/spefsa.2024.EN-9049 by Istuito Zogorofilatico Sperimena dell'Umbria e delle Marche (IZSUM), Wiley Online Library on 1041 2020/J. See the Terms and Conditions (https://minielibrary.wiley.com/drions) on Wiley Online Library for rules of use; OA articles are govered by the applicable Cereative Commons



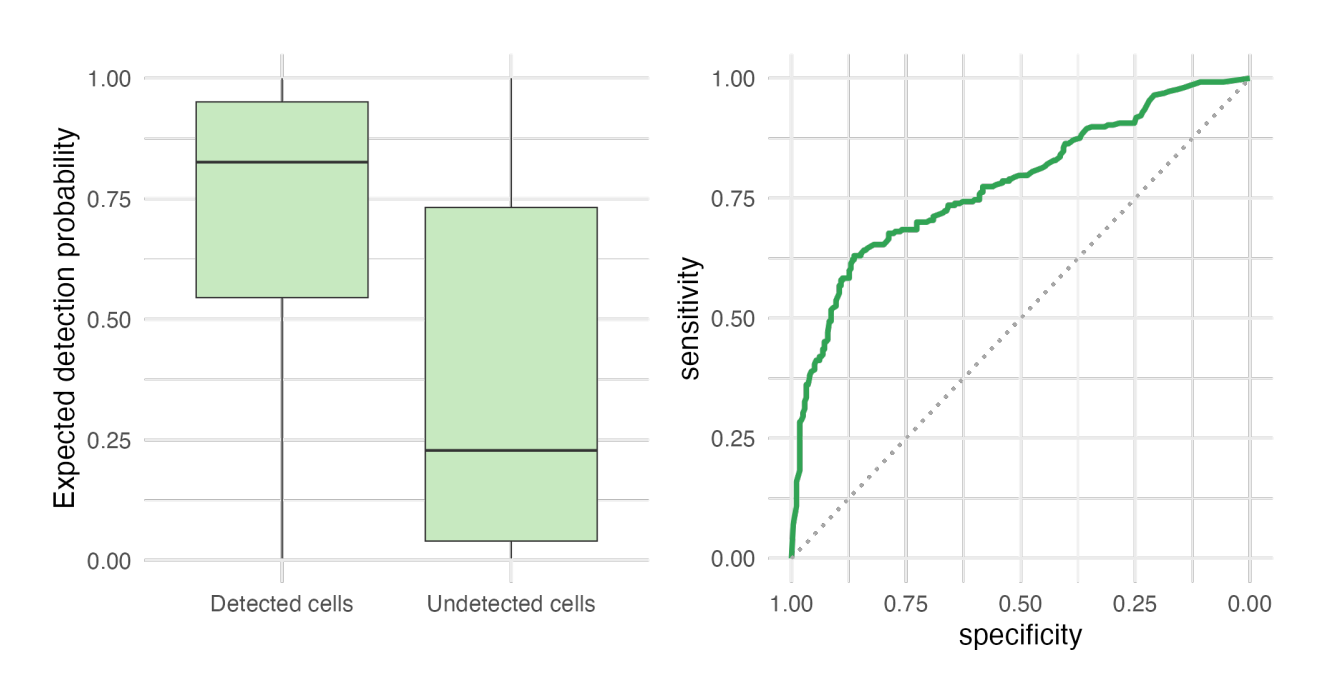


Figure 9. Ability of the model to discriminate between detected and non-detected cells. (Left) Expected detection probability, as calculated by the best-fitting model, for cells that were actually detected or not, as informed by the surveillance data provided by EFSA. (Right) Receiver operating characteristic (ROC) curve comparing the probability of detection of infectious cells, as calculated by the model, against the observed detection status, as informed by the surveillance data provided by EFSA. The area under the curve (AUC) was 0.78, corresponding to a moderate ability of the model to discriminate between cells that were correctly detected as infected and those that were not.

3.5 Density assessment

As mentioned above, the overall influence of wild boar density on explaining observed ASF transmission patterns was evaluated across the whole study period through comparing model performance. The best-fitting model used a seasonal transmission rate without modulating cell susceptibility or infectivity based on density, indicating that wild boar density did not play a role in better-informing observed transmission patterns when examined en-masse across the entire study period (January 2022 - September 2023). To refine this assessment, we evaluated if the effect of density differed between epidemic waves. In the first wave, the proportion of higher-density detected cells in the observed data (those above the study area median density of 5.7 wild boar/km²) fell within the 95% prediction interval of the expected proportion of higher-density cells that would be detected under the null scenario (where there is no density effect) (0.55 and 0.64, respectively) (Figure 10). Conversely, in the second wave, the observed proportion of higher-density detected cells (0.60) fell outside the 95% prediction interval of the null scenario (0-0.58), suggesting that a statistically significant effect of density was observed in the second wave.





37832, 2024, 1, 1, Dowlondedd from https://efsa.onlinelblary.wisley.comdroi/10.2903/sep.fea.2024.EN-9049 by Istituto Zoprofoliatics Sperimena del Umbria e delle Marche (LZSUM), Wiley Online Library on (04/12/2024). See the Terms and Conditions (https://onlinelblary.wisley.com/terms-and-conditions) on Wiley Online Library for rules of use; OA articles are govered by the applicable Creative Commons



The growth rate of the spatial extent of the total infected area (defined by those cells contained within a minimum convex polygon encapsulating all infected cells up to that week) was determined per week over the course of the study period using the model not accounting for an effect of density (Figure 11). Epidemic progression rates were observed to vary seasonally, in accord with the seasonally-variable transmission rate in the model. In the first wave, the maximum rate of growth was seen in February (2022) with an average monthly median value of 44 km² per week (CI₉₅ 0, 132), while the minimum rate of growth was seen in July (2022) with an average monthly median value of 0 km² per week (CI₉₅ 0, 36). In the second wave, the maximum rate of growth was seen in January (2023) with an average monthly median value of 124 km² per week (CI₉₅ 29, 268), while the minimum rate of growth was seen in June (2023) with an average monthly median value of 0km² per week (CI₉₅ 0, 52).

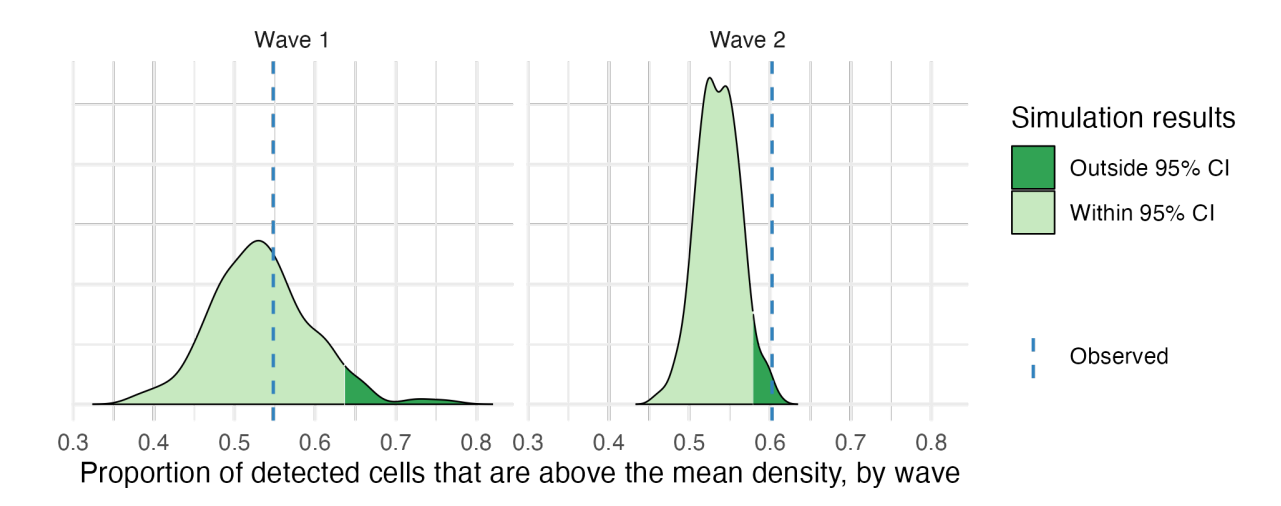


Figure 10. Proportions of detected cells that are above the median density of the study area for the observed data and simulated data from the null scenario. In the first wave, the observed proportion of detected cells that were above the mean density (blue dashed line) fell within the 95% credible interval for the proportion of detected cells above the mean density that would be expected under the null scenario (light-green shaded region of distribution). In the second wave, the observed proportion of higher-density detected cells fell outside of the 95% credible interval for the null scenario (dark-green shaded region). This indicates that, in the second wave, the proportion of higher-density detected cells is higher than that which would be expected under the scenario where density does not have an effect, and thus a significant effect of density was seen in this wave.





ded from https://efs.aonlinelibary.wikey.com/doi/10.2993/sp.efsa.2024.EN-9049 by Istituto Zooprofilatico Sperimentad ell'Umbria e delle Marche (IZSUM), Wikey Online Library on [04/12/2024]. See the Terms and Conditions (https://omlehibrary.wiley.com/terms-and-conditions) on Wiley Online Library for rules of tase; Os Aarticles are governed by the applicable Cereive Commons



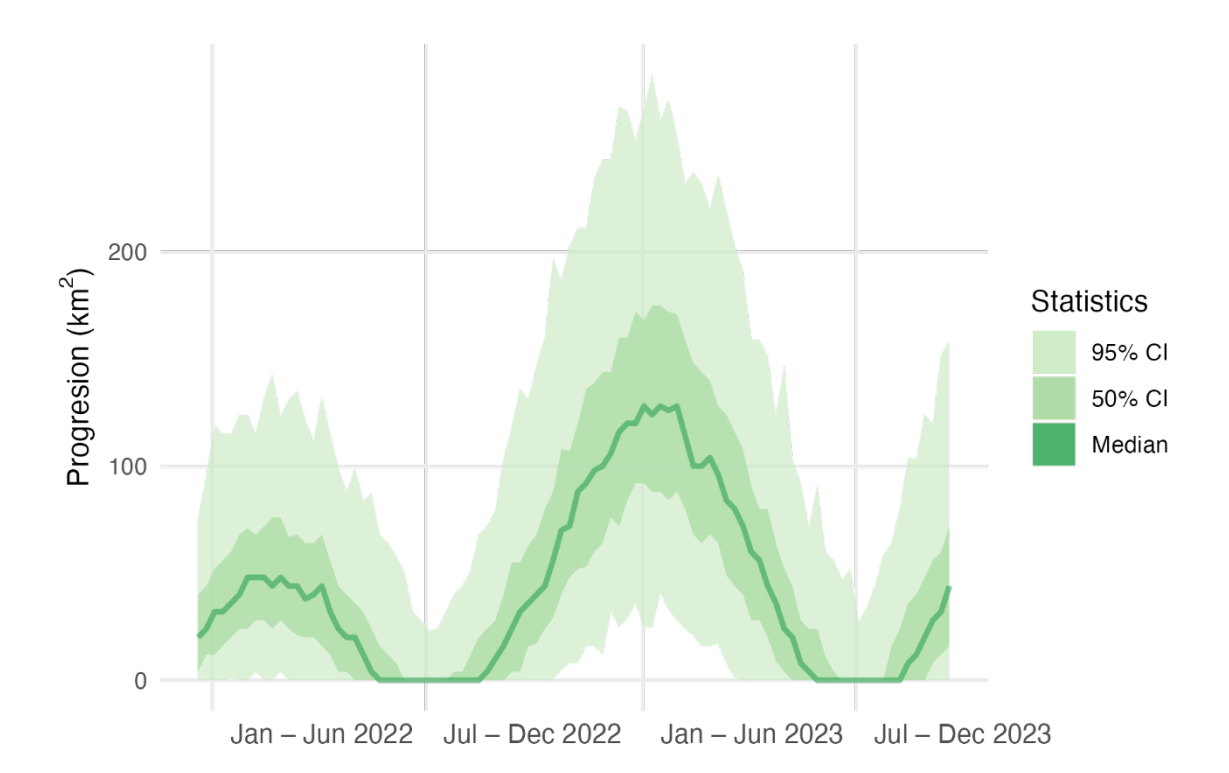


Figure 11. Weekly growth rates of the infected area (n.b. not only detected cells, but all infected cells), across all simulations, using the model not accounting for an effect of density. The weekly growth rate is defined as the difference in size of the affected area between a week and the preceding week. The light green ribbon indicates 95% credible intervals (CI95), the dark green ribbon indicates 50% credible intervals, and the darkest green line indicates median values. In the first wave, the maximum rate of growth is seen in February with an average monthly median value of 44 km² per week (CI95 0, 132), while the minimum rate of growth is seen in July with an average monthly median value of 0 km² per week (CI₉₅ 0, 36). In the second wave, the maximum rate of growth is seen in January with an average monthly median value of 124 km² per week (CI95 29, 268), while the minimum rate of growth is seen in June with an average monthly median value of 0 km² per week (CI₉₅ 0, 52).

4 Discussion

Elucidating the relationship between ASF transmission and wild boar density is a key component for developing improved control strategies (Guberti et al., 2022). Previous research suggested associations between ASF prevalence and wild boar density, however it was possible that the observed relationships were confounded by the effects of on-going control measures (Nurmoja et al., 2017; Schulz et al., 2019). Here, by using high-quality surveillance data and relying on carefully-chosen model assumptions, we managed to fit a simple mechanistic model to the two-wave epidemic of ASF that occurred in Northern Italy between January 2022 and September 2023. In doing so, we found that a wild boar density effect was not informative in explaining the overall observed transmission pattern across the 21-month period. However, the data suggested an effect of density during the second wave only. The apparent lack of an influence of density in the transmission pattern of the first wave

www.efsa.europa.eu/publications







397832,5. 2024, 11, Downloaded from https://efsa.onlinelibrary.wiley.com/drio/10.2903/spefsa.2024.EN-9049 by Istuito Zogorofilatico Sperimena dell'Umbria e delle Marche (IZSUM), Wiley Online Library on 1041 2020/J. See the Terms and Conditions (https://minielibrary.wiley.com/drions) on Wiley Online Library for rules of use; OA articles are govered by the applicable Cereative Commons



could be the result of a lack of power due to the fact that the first wave was observed for only a 38-week period, as opposed to the full 52-week period seen in the second wave. Additionally, the surveillance outcomes were not equal between the two waves. During the first wave, 771 carcasses were located (averaging 20.3 carcasses per week), while during the second wave 1503 carcasses were located (averaging 28.9 carcasses per week), over approximately the same surface area. The lower surveillance rate seen during the first wave could also be a contributing factor to the apparent lack of influence of density, depending on the methods guiding the surveillance efforts. Analysing the subsequent wave (September 2023 through October 2024) could be useful for refining this assessment. Further, it must be kept in mind that the wild boar abundance estimates that were used as a model input refer to the period prior to ASF emergence. It is probable that the wild boar abundance distribution across the study period when the second wave started (September 2022) no longer reflected the assumed distribution, introducing a potential bias in the analysis. To better characterise the wave-specific impact of wild boar density, it would be beneficial to conduct further investigations by extending the mechanistic model used in this study to estimate parameters for individual epidemic waves.

In our model, we examined epidemic trajectories across multiple years and included the capability for habitat reinfection events. However, wild boar density was assumed to be constant across the study period, though this is known to not be the case following an ASF incursion where upwards of 95% of the wild boar population will die (European Food Safety Authority (EFSA) et al., 2018). Better characterisation of local wild boar population dynamics during an ASF epidemic, and including density estimates both pre- and post-ASF introduction may allow more accurate modelling of reinfection across years, as well as permit the model to be applied to areas where ASF is already endemic.

In addition to explaining transmission patterns, wild boar density may also play a role in dictating if ASF can successfully establish itself in a new region. Reducing and stabilising the wild boar density of a region prior to the introduction of ASF has been suggested as a preventive measure, but as explicit density thresholds that permit successful ASF introduction and establishment are unknown, so too is the target density for density reduction efforts (European Food Safety Authority (EFSA) et al., 2018). In northern Italy the minimum estimated wild boar density of the study region was 2.5 individuals/km², though field studies have shown the ASF virus to be successful at infecting and persisting in areas of far lower density (e.g. Poland, where there were less than 0.4 wild boar/km²) (Pejsak et al., 2014). Parameterising the model to other epidemic scenarios where there are far lower wild boar densities may serve to further inform the influence of density on epidemic dynamics.

Though we have relative evidence that density plays a role in shaping ASF transmission patterns in emergent scenarios, the role of wild boar density in explaining endemicity still requires investigation. Theoretical modelling studies that have evaluated endemicity mechanisms indicate that even at densities of 1.5 individuals/km², ASF could persist for at least 10 years (Gervasi & Guberti, 2021). Adapting the present model to endemic scenarios (along with accounting for post-ASF introduction wild board density decreases), and then

www.efsa.europa.eu/publications







led from https://efsa.onfinelibrary.wiley.com/doi/10.2903/sp. efsa. 2024.EN-9049 by Istituto Zooproflattico Sperimenta ed Il'Umbria e delle Marche (IZSUM), Wiley Online Library on [04/1/2/2024]. See the Terms and Conditions) on Wiley Online Library for rules of use; OA articles are govered by the applicable Ceretive Commons



fitting it to the observed data of EU member states where ASF is considered endemic, could provide insight into the role of density in endemic establishment.

Assumptions were necessary at multiple stages of model development. To reconstruct infectious periods, carcasses were assumed to remain infectious for an average of 4 or 6 weeks after death (depending on the season). Carcass contact is an established driver of transmission, and carcasses have been shown to be capable of remaining infectious for up to several months (Fischer et al., 2020; Probst et al., 2017). Utilising carcass persistence data specific to the modelled region would allow more reliable estimation of true infectious periods. Indeed, when examining reinfection rates among the observed data, half were seen to occur within the same wave as the previous infection. In the first wave especially, using our defined infectious periods, reinfection events occurred a median of two weeks apart. Realistically this is an artifact of assumed persistence of carcass infectiousness, and the apparently reinfected cells were likely truly infectious across both periods. These reinfection events inflate the calculated observed cell-level weekly incidence, and in the simulated data, wave one infections were fewer than in the observed data. Re-estimating infectious periods to avoid these artifacts and re-fitting the model may provide more refined parameter estimates, especially relating to the first epidemic wave.

Seasonal periods had to be defined to inform carcass persistence, and in our model, we chose a simple binary partition: winter and non-winter. Ideally more complex variation in the effects of seasonality that impacts carcass persistence would be included to better reflect real-world dynamics, but for the purposes of our model we felt this partition was sufficient.

5 Conclusions and recommendations

- The mechanistic model that was described here successfully captured the temporal and spatial trends of the ASF epidemic that occurred in Northern Italy between January 2022 and September 2023.
- The epidemic under study did not support a wild boar density effect on ASF spread enmasse across the study period, but rather suggests a wave-specific effect with wild boar density having shaped ASF spread only during the second wave (October 2022 -September 2023).
- The model used in this study could be extended and adjusted to the individual epidemic waves (including the third one), to clarify the mechanisms linking wild boar density and observed ASF epidemic trajectories.
- This model could be explored further to investigate wild boar density thresholds that would allow natural fade-outs of ASF spread, if such non-zero thresholds exist.
- Further, it would be beneficial to validate these results against other contexts of ASF emergence (e.g. Belgium, Germany, Sweden), to determine if an influence of wild boar density is present across epidemic scenarios.





37852, 2024. 1. Dowlwaded from thes://esa.oninelbrary.wie.e.com/doi/10.2903/sp. efsa.2024.EN-9949 by Istituto Zooprofilatico Sperimenta dell'Umbria e delle Marche (IZSUM), Wely Online Library of 04/12/2024, See the Terms and Conditions (https://onlinelbrary.wie.e.com/embriary.wi



- Agenzia regionale per la protezione ambientale (ARPA) Liguria. (2024). Weather and climate regional data [Dataset]. https://www.arpal.liguria.it/
- Agenzia regionale per la protezione ambientale (ARPA) Lombardia. (2024). Weather and climate regional data [Dataset]. https://www.arpalombardia.it/
- Agenzia regionale per la protezione ambientale (ARPA) Piemonte. (2024). Weather and climate regional data [Dataset]. https://www.arpa.piemonte.it/
- Blome, S., Gabriel, C., & Beer, M. (2013). Pathogenesis of African swine fever in domestic European wild boar. Virus Research, 173(1), https://doi.org/10.1016/j.virusres.2012.10.026
- ENETWILD consortium. (2024). Modelling wild boar abundance at high resolution. EFSA Supporting Publications, 21(7), 8965E. https://doi.org/10.2903/sp.efsa.2024.EN-8965
- European Food Safety Authority (EFSA), Butterworth, A., Calistri, P., Edwards, S., Garin-Bastuji, B., Good, M., Michel, V., Raj, M., Nielsen, S. S., Sihvonen, L., Spoolder, H., Stegeman, J. A., Velarde, A., Willeberg, P., Winckler, C., Depner, K., Guberti, V., Masiulis, M., Olsevskis, E., ... Gortázar Schmidt, C. (2018). African swine fever in wild boar. EFSA Journal. Food European Safety Authority, 16(7), e05344. https://doi.org/10.2903/j.efsa.2018.5344
- Fischer, M., Hühr, J., Blome, S., Conraths, F. J., & Probst, C. (2020). Stability of African Swine Fever Virus in Carcasses of Domestic Pigs and Wild Boar Experimentally Infected with the ASFV "Estonia 2014" Isolate. Viruses, 12(10), 1118. https://doi.org/10.3390/v12101118
- Gervasi, V., & Guberti, V. (2021). African swine fever endemic persistence in wild boar populations: Key mechanisms explored through modelling. Transboundary and Emerging Diseases, 68(5), 2812-2825. https://doi.org/10.1111/tbed.14194
- Gillespie, D. T. (2001). Approximate accelerated stochastic simulation of chemically reacting The Journal Chemical Physics, 115(4), 1716-1733. systems. of https://doi.org/10.1063/1.1378322
- Grimm, V., Berger, U., Bastiansen, F., Eliassen, S., Ginot, V., Giske, J., Goss-Custard, J., Grand, T., Heinz, S. K., Huse, G., Huth, A., Jepsen, J. U., Jørgensen, C., Mooij, W. M., Müller, B., Pe'er, G., Piou, C., Railsback, S. F., Robbins, A. M., ... DeAngelis, D. L. (2006). A standard protocol for describing individual-based and agent-based models. Ecological Modelling, 198(1), 115-126. https://doi.org/10.1016/j.ecolmodel.2006.04.023
- Grimm, V., & Railsback, S. F. (2012). Pattern-oriented modelling: A 'multi-scope' for predictive systems ecology. Philosophical Transactions of the Royal Society B: Biological Sciences, 367(1586), 298-310. https://doi.org/10.1098/rstb.2011.0180
- Grimm, V., Railsback, S. F., Vincenot, C. E., Berger, U., Gallagher, C., DeAngelis, D. L., Edmonds, B., Ge, J., Giske, J., Groeneveld, J., Johnston, A. S. A., Milles, A., Nabe-Nielsen, J., Polhill, J. G., Radchuk, V., Rohwäder, M.-S., Stillman, R. A., Thiele, J. C., & Ayllón, D. (2020). The ODD Protocol for Describing Agent-Based and Other Simulation Models: A Second Update to Improve Clarity, Replication, and Structural Realism. Journal of Artificial Societies and Social Simulation, 23(2), 7.
- Guberti, V., Khomenko, S., Masiulis, M., & Kerba, S. (2022). African swine fever in wild boar - Ecology and biosecurity (2nd ed.). FAO; World Organisation for Animal Health (WOAH); European Commission.





10.2002. Deep training the properties of the pro



- Guinat, C., Porphyre, T., Gogin, A., Dixon, L., Pfeiffer, D. U., & Gubbins, S. (2018). Inferring within-herd transmission parameters for African swine fever virus using mortality data from outbreaks in the Russian Federation. Transboundary and Emerging Diseases, 65(2), e264e271. https://doi.org/10.1111/tbed.12748
- Hayes, B., Lim, J-S., Andraud, Mathieu & Vergne, T. (2024). Supplementary material of the stochastic model to elucidate the influence of wild boar density on African swine fever boar populations, spread wild Zenodo. https://doi.org/10.5281/zenodo.14002930
- Jabot, F., Faure, T., Dumoulin, N., & Carlo Albert. (2023). EasyABC: Efficient Approximate Bayesian Computation Sampling Schemes (Version 1.5.2) [R]. https://CRAN.Rproject.org/package=EasyABC
- Keeling, M. J., & Rohani, P. (2008). Stochastic Dynamics. In Modeling Infectious Diseases in Humans and Animals (pp. 190-231). Princeton Press. https://doi.org/10.2307/j.ctvcm4gk0
- Lenormand, M., Jabot, F., & Deffuant, G. (2012). Adaptive approximate Bayesian computation for complex models. https://hal.archives-ouvertes.fr/hal-00638484
- Lim, J.-S. (2024, May). Estimated delay durations in detection of wild boar carcasses in South Korea. [Personal communication].
- Nurmoja, I., Schulz, K., Staubach, C., Sauter-Louis, C., Depner, K., Conraths, F. J., & Viltrop, A. (2017). Development of African swine fever epidemic among wild boar in Estonia—Two different areas in the epidemiological focus. Scientific Reports, 7(1), 12562. https://doi.org/10.1038/s41598-017-12952-w
- Pebesma, E. (2018). Simple Features for R: Standardized Support for Spatial Vector Data. The R Journal, 10(1), 439–446.
- Pejsak, Z., Truszczyński, M., Niemczuk, K., Kozak, E., & Markowska-Daniel, I. (2014). Epidemiology of African Swine Fever in Poland since the detection of the first case. Polish Journal of Veterinary Sciences, 17(4), 665-672. https://doi.org/10.2478/pjvs-2014-0097
- Pietschmann, J., Guinat, C., Beer, M., Pronin, V., Tauscher, K., Petrov, A., Keil, G., & Blome, S. (2015). Course and transmission characteristics of oral low-dose infection of domestic pigs and European wild boar with a Caucasian African swine fever virus isolate. Archives of Virology, 160(7), 1657–1667. https://doi.org/10.1007/s00705-015-2430-2
- Probst, C., Globig, A., Knoll, B., Conraths, F. J., & Depner, K. (2017). Behaviour of free ranging wild boar towards their dead fellows: Potential implications for the transmission of fever. 4(5), African swine Royal Society Open Science, 170054. https://doi.org/10.1098/rsos.170054
- R Core Team. (2024). R: A language and environment for statistical computing. (Version 4.4.1 "Race for Your Life") [Computer software]. R Foundation for Statistical Computing. https://www.R-project.org/
- Schulz, K., Staubach, C., Blome, S., Viltrop, A., Nurmoja, I., Conraths, F. J., & Sauter-Louis, C. (2019). Analysis of Estonian surveillance in wild boar suggests a decline in the incidence of African swine fever. Scientific Reports, 9(1), 8490. https://doi.org/10.1038/s41598-019-44890-0
- Tennekes, M. (2018). tmap: Thematic Maps in R. Journal of Statistical Software, 84, 1-39. https://doi.org/10.18637/jss.v084.i06







3.978325, 2024.11, Downwaled from https:///sta.onlinelbury.wikey.com/doi/10.29036, peksa.2024.EN-9049 by Istituto Zooprofilatics Sperimenta dell'Umbria e delle Marche (IZSUM), Wiley Online Library on [04/12/2024]. See the Terms and Conditions (https://onlinelbury.wikey.com/doi/10.29036, peksa.2024.EN-9049 by Istituto Zooprofilatics Sperimenta dell'Umbria e delle Marche (IZSUM), Wiley Online Library on [04/12/2024]. See the Terms and Conditions (https://onlinelbury.wikey.com/doi/10.29036, peksa.2024.EN-9049 by Istituto Zooprofilatics Sperimenta dell'Umbria e delle Marche (IZSUM), Wiley Online Library on [04/12/2024]. See the Terms and Conditions (https://onlinelbury.wikey.com/doi/10.29036, peksa.2024.EN-9049 by Istituto Zooprofilatics Sperimenta dell'Umbria e delle Marche (IZSUM), Wiley Online Library on [04/12/2024]. See the Terms and Conditions (https://onlinelbury.wikey.com/doi/10.29036, peksa.2024.EN-9049 by Istituto Zooprofilatics Sperimenta dell'Umbria e delle Marche (IZSUM), Wiley Online Library on [04/12/2024]. See the Terms and Conditions (https://onlinelbury.wikey.com/doi/10.29036, peksa.2024.EN-9049 by Istituto Zooprofilatics Sperimenta dell'Umbria e delle Marche (IZSUM), Wiley Online Library on [04/12/2024]. See the Terms and Conditions (https://onlinelbury.wikey.com/doi/10.29036, peksa.2024.EN-9049 by Istituto Zooprofilatics (https://onlinelbury.wikey.com/doi/10.29036, peksa



Wickham, H., Averick, M., Bryan, J., Chang, W., McGowan, L. D., François, R., Grolemund, G., Hayes, A., Henry, L., Hester, J., Kuhn, M., Pedersen, T. L., Miller, E., Bache, S. M., Müller, K., Ooms, J., Robinson, D., Seidel, D. P., Spinu, V., ... Yutani, H. (2019). Welcome Tidyverse. Journal of Open Source Software, 4(43), https://doi.org/10.21105/joss.01686





3978325, 2024, 11, Downloaded from https://efsa.onlinelibrary.wiley.com/doi/10.2903/sp.efsa.2024.EN-9049 by Istituto Zooprofilatico Sperimenta dell'Umbria e delle Marche (IZSUM), Wiley Online Library on 104/12/2024. See the Terms

and-conditions) on Wiley Online Library for rules of use; OA articles are governed by the applicable Creative Commons



Abbreviations

ABC Approximate Bayesian computation **APMC** Adaptive population Monte Carlo

ASF African swine fever 95% credible interval CI₉₅

EFSA European Food Safety Authority infectious-undetected infection state I_{u} \mathbf{I}_{d} infectious-detected infection state ODD Overview, Design concepts, Details

R Recovered infection state S Susceptible infection state

SIRS Susceptible-Infectious-Recovered-Susceptible

SMC Sequential Monte Carlo







ded from https://efs.aonlinelibary.wikey.com/doi/10.2993/sp.efsa.2024.EN-9049 by Istituto Zooprofilatico Sperimentad ell'Umbria e delle Marche (IZSUM), Wikey Online Library on [04/12/2024]. See the Terms and Conditions (https://omlehibrary.wiley.com/terms-and-conditions) on Wiley Online Library for rules of tase; Os Aarticles are governed by the applicable Cereive Commons



APPENDIX A - ODD (Overview, Design concepts, Details)

A.1. Overview

The ASF wild boar density assessment model, an agent-based mechanistic model of African swine fever (ASF) transmission across a density-explicit wild boar habitat grid, was developed through a pattern-oriented modelling approach (Grimm & Railsback, 2012). It is a model composed of two sub-models, one for parameter calibration and another for parameter evaluation, each of which are comprised of smaller modules for executing specific functions. The model description follows the ODD (Overview, Design concepts, Details) protocol for describing individual- and agent-based models (Grimm et al., 2006), as updated by Grimm et al. (2020).

A.1.1. **Purpose and patterns**

The purpose of the model is to investigate the impact of wild boar density in explaining the observed spatiotemporal transmission patterns of ASF using density-explicit wild boar habitat cells. The model is evaluated by its ability to reproduce observed epidemiological patterns in ASF weekly incidence and spatial spread.

A.1.2. **Entities, state variables, and scales**

A.1.2.1 **Entities**

The entities in the model are contiguous 2 km x 2 km grid cells of wild boar habitat containing explicit density estimates, representative of real-world locations (see §A.3.1 for details).

State variables A.1.2.2

Each cell tracks three state variables: identification (ID), relative wild boar density, and infection state (Table A.1). Each cell receives a unique integer for identification. Wild boar density estimates (previously estimated, see §A.3.1 for details) are assumed to be constant, and are given as positive floating-point numbers. Infection states follow a detection-delay SIR mechanistic epidemiological model, with cells cycling through four possible states of infection: susceptible (S), infectious-undetected (I_u), infectious-detected (I_d), and recovered (R), with the potential to return to the susceptible state following recovery. Latency was not considered as the model operates on a geographic (as opposed to individual) scale with cell infectious periods of at least four weeks (see §A.3.4.1.1(iii) for details), and the 2-4 day latent period of ASF in wild boar was considered to have a negligible contribution to overall dynamics (Blome et al., 2013; Pietschmann et al., 2015).

A.1.2.3Scales

The spatial and temporal scales of the model are subject to the inputted data. The spatial extent is defined by the largest detected case cluster, and duration of model is determined by the temporal range of surveillance data within that cluster (see §A.3.1 for further detail)

www.efsa.europa.eu/publications







ded from https://efsa.onlinelibaray.wiley.com/doi/10.2903/sp. efsa. 2024.EN-9049 by Istituto Zooprofilative Sperimenta dell'Umbria e delle Marche (IZSUM), Wiley Online Library on [04/12/2024]. See the Terms and Conditions (https://onlinelibrary.wiley.com/terms-and-conditions) on Wiley Online Library for rules of use; e. C. articles are govered by the applicable Ceretive Commons



Table A.1. Cell state variables

Cell state variable	Characteristics
Identification	Unique numeric value assigned to each cell
Wild boar density	Estimate of wild boar per square kilometer within that cell.
Infection state	Infectious status of a cell: susceptible, infectious- undetected, infectious-detected, or recovered.

A.1.1. **Process overview and scheduling**

A.1.1.1. Process overview

The model was developed to capture the observed epidemiological detection pattern in real ASF surveillance data over a multiyear period using a density-explicit cellular grid of the study area. Achieving this outcome requires the use of multiple models, where each model is defined by the employed combination of transmission parameters (see §A.3.2 for further detail). For each model, two sequential processes occur in distinct sub-models: parameter calibration and parameter testing. In the calibration sub-model, particles of transmission parameters are estimated via adaptive population Monte Carlo (APMC), a variant of sequential Monte Carlo approximate Bayesian computation schemes (ABC-SMC) (see §A.3.4.1.4(vi) for details) (Lenormand et al., 2012). In the evaluation sub-model, data is simulated from the particle set (that is, sets of conserved values for the included parameters) for the corresponding model (transmission parameter combination). Within both these sub-models, the data structures that drive the simulation module are generated from observed data, and are then used to execute the epidemic simulation module. The parameter combination that provides the closest fit to the data is used to define the best-fitting model, and the data simulated from the best-fitting model is used to investigate the research question.

A.1.1.2. Schedule

The epidemic simulation module proceeds in weekly time steps. Within-simulation processes infection, detection, recovery, and re-susceptibility-are performed at each time step as applicable (see §A.3.4.1.4(v) for further detail).

A.2. Design concepts

A.2.1. **Basic principles**

The basic principle behind the model is that ASF spread among wild boar will be seen to spread near-contiguously through interconnected wild boar habitat in a highly-surveilled environment. Through calibrating transmission parameters to this observed process, these dynamics can be replicated. At a system level, this model addresses the question of whether wild boar density estimates are informative in explaining observed ASF transmission patterns, through yielding results of simulations that both include and exclude parameters to modulate the effect of density on disease transmission. Here, these transmission parameters consist of a transmission rate, relative susceptibility of cells based on wild boar density, and relative infectivity of cells based on wild boar density. Through evaluating the outcomes of multiple

www.efsa.europa.eu/publications







ded from https://efsa.onlinelibrary.wiley.com/doi/10.2903/sp.efsa.2024.EN-9049 by Istituto Zooprofilattico Sperimenta dell'Umbria e delle Marche (IZSUM), Wiley Online Library on [04/1/2/2024]. See the Terms and Conditions (https://onlinelibrary.wiley.com/terms

-and-conditions) on Wiley Online Library for rules of use; OA articles are governed by the applicable Creative Commons



models that reflect all available combinations of transmission parameters, the influence of wild boar density on explaining observed transmission patterns can be elucidated.

A.2.2. **Emergence**

From the simulation module emerges a spatiotemporal pattern of both apparent (infectious detected) and true (infectious undetected) simulated incidence of ASF transmission across wild boar habitat, to be contrasted to the pattern seen in the observed (i.e. observed in the real-world) data. The pattern is analysed in terms of weekly incidence, spatial extent, and probability of detection per cell. Patterns in ASF detection and recovery can also emerge, though such patterns would be tightly constrained to the observed data that informs those processes.

A.2.3. Interaction

Interaction exists only between neighbouring cells, and reflects the infectious pressure exerted by infectious cells upon susceptible cells. The ability to undergo this interaction is determined by the Moore neighbourhood of each cell.

A.2.4. Stochasticity

Stochasticity is included in the infection, detection, and recovery processes to reflect biological variability. The process to return to the susceptible state is deterministic and aligned to the observed epidemic waves.

A.2.5. **Observation**

Simulation behaviour is observed through an infection state summary table that tracks the week of each infection state change for all cells that undergo infection state changes. During the calibration phase, the model is observed through summary statistics that reflect temporality (incidence), spatial extent (the area of the minimum convex polygon around detected cells), and density (the total wild boar density of infectious-detected cells) per period. During the parameter evaluation phase, the model returns the state matrix summary for each particle (parameter set) tested. From here, both apparent (detected) and true (all infections) simulated weekly incidence are able to be examined alongside the incidence of the real-world observed data. The probability of detection of cells for both the apparent and true simulated data is calculated for all cells and viewed spatially alongside the real observed data.

Adaptation, objective, learning, sensing and interaction processes are not implemented, nor does the model include any collectives.

A.3. Details

A.3.1. **Data preparation**

The ASF wild boar density assessment model is constructed from spatially-explicit ASF surveillance data and spatially-explicit gridded wild boar density estimate data. ASF carcass

www.efsa.europa.eu/publications







397832,5. 2024, 11, Downloaded from https://efsa.onlinelibrary.wiley.com/drio/10.2903/spefsa.2024.EN-9049 by Istuito Zogorofilatico Sperimena dell'Umbria e delle Marche (IZSUM), Wiley Online Library on 1041 2020/J. See the Terms and Conditions (https://minielibrary.wiley.com/drions) on Wiley Online Library for rules of use; OA articles are govered by the applicable Cereative Commons



surveillance data is provided by the European Food Safety Authority (EFSA), and contains information for date of carcass detection, method of detection (found dead, hunted, or road/predator killed), ASF virus polymerase chain reaction (PCR) laboratory result for the tested carcass (positive or negative), and the explicit coordinates of the carcass location. This data is used to identify and delineate the region and period of study. A country is selected, and ASF case clusters are identified through nearest-neighbourhood contiguity of found-dead wild boar carcasses, assuming a maximum local transmission distance of 20 km between related cases. A minimum convex polygon around the largest case cluster plus a 20 km buffer defines both the study region the spatial scale of the model.

The ENETWILD consortium previously estimated wild boar distribution and abundance throughout Europe as a discrete-space two-dimensional cell grid at 4 km² resolution, with each cell containing the estimated number of individual boar per square kilometer (ENETWILD consortium, 2024). The cells located within the study region are extracted to comprise the local wild boar habitat grid. Surveillance data is binned per cell and estimated infectious periods are calculated at the cell level (see §A.3.4.1.1(iii) for details). Epidemic waves are determined through visualisation of weekly incidence, and the surveillance data is truncated to the end of the last complete epidemic wave. The end of an epidemic wave is assumed to be annually cyclical and is defined as the week of a period in which no new cells are detected as infected, that is present across all years of study. A new minimum convex polygon around the final surveillance dataset is generated with a 20 km buffer, and the cells located within the new study region are extracted to comprise the local wild boar density habitat grid. The surveillance data is intersected with the new study area to update the cell IDs for each surveillance event. The surveillance and density grid datasets are now ready to be fed into the model.

A.3.2. **Initialisation**

The model is initialized and ran on a computing cluster via a bash script. The bash script ("submit_jobs_full.sh" or "submit_jobs_toy.sh", depending on whether the full model or a smaller toy model is to be ran) is written for a computing cluster that is managed by the Sun Grid Engine batch-queuing system. The bash script is to be submitted from the home directory of the project, with the project itself located within the R folder (~/R/efsa_asf). In the job submission script, model variables are specified for whether or not the toy model is to be ran ("toy"), the duration of the assumed delay between infection and detection for wild boar carcasses ("inf_to_det_delay", default value of 4 [weeks]), and a vector of which weeks of the year qualify as belonging to the winter period ("winter_weeks", default value of weeks 1-6 and 49-52). Combinations of included parameters that reflect all eight combinations of transmission rate formulation and inclusion of relative susceptibility and/or infectivity parameters are generated as well, and each model is assigned a unique submission number between 1 and 8 (see Table A.2 for correspondence between model (submission) identification number and included parameters). With this information, all eight models are submitted to the queuing system and ran in parallel. Model variables (e.g. which parameters are to be included, and infection to detection delay), are exported to the system environment.





ded from https://efsa.onlinelibrary.wilety.com/doi/10.2903/sjp.efsa.2024.EN-9049 by Istituto Zooprofilattico Sperimenta dell'Umbria e delle Marche (IZSUM), Wiley Online Library on [04/12/2024]. See the Terms and Conditions) on Wiley Conline Library for rules of use; OA articles are governed by the applicable Ceretive Commons



If desired, one can input their email in the bash script (where indicated) to receive email updates on job progress.

The bash script, to be ran from the parent directory "/efsa_asf" calls the file "scripts/02run_model.R". Here, all exported variables are imported into the R session to parameterise the model.

Table A.2. Parameters included in each model, by model identification number

Identification number	Transmission rate	Relative susceptibility	Relative infectivity
1	Constant β	Excluded	Excluded
2	Constant β	Included	Excluded
3	Constant β	Excluded	Included
4	Constant β	Included	Included
5	Seasonal β	Excluded	Excluded
6	Seasonal β	Included	Excluded
7	Seasonal β	Excluded	Included
8	Seasonal β	Included	Included

A.3.3. Input data

Input data required to drive the disease state processes is derived from the surveillance and wild boar density grid data that was generated in "scripts/01-data_prep.R" (§A.3.1). The files "dat_surv_italy.rds" and "dat_wb_grid_italy.rds", from the aforementioned script are used to compute cell infectious periods, per-cell weekly detection rates, seasonal recovery rates, weeks which an epidemic wave ends, the contact index between cells that permits transmission, and which cells are to initialise the epidemic (§A.3.4.1.1). Additional input data, namely the number of simulations to be used in each generation of particle estimation and the week aggregation over which summary statistics are to be assessed (default of 12 week periods), are hardcoded in the parent script ("scripts/02-run_model.R")

A.3.4. Sub-models

The ASF wild boar density assessment model consists of two sub-models contained in the parent script "scripts/02-run_model.R": the APMC parameter calibration sub-model and the parameter testing sub-model. The first sub-model—parameter calibration—relies on prior distributions for input and returns a set of particles that best reproduce the observed data (along with other ABC-SMC metrics). Following calibration, the second sub-model—parameter testing—commences by extracting the conserved particle set and run one simulation for each particle. A summary of the state transitions of each cell is returned, which is then appended to the output of the first sub-model and saved as the file "data/gen/results_model_#.rds", with # indicating the model identification number (1-8) given during job submission. Once the output for all models is obtained (results_model_1.rds through results_model_8.rds), they should be transferred locally where the script "scripts/03-analysis.R" can be used on the





led from https://efsa.on/inel/brary.wiley.com/doi/10.2903/sp. efsa. 2024.EN-9049 by Istituto Zooprofilattico Sperimenta ed Il'Umbria e delle Marche (IZSUM), Wiley Online Library on [0.41/2.2024]. See the Terms and Conditions) on Wiley Online Library on rules of use; OA articles are governed by the applicable Ceretive Commons



results. The following modules, within the sub-models, are presented in the order in which they are executed.

A.3.4.1. APMC calibration sub-model

The calibration sub-model generates required data structures, generators parameter posterior distributions, calculates summary statistics of the observed data, and then runs the simulation.

A.3.4.1.1. Generate input data structures

The script "scripts/02.1-InitSim.R" is called, which provides a function that uses the variables brought in from the environment (toy model status, infection to detection delay, and vector of winter weeks) to generate necessary model data structures.

(i) Surveillance and density data

The observed data—both the surveillance data of the region ("data/gen/dat_surv_italy.rds") and the wild boar density grid ("data/gen/dat_wb_grid_italy.rds")—is brought into the system environment. For each surveillance event, the relative week within the model is calculated. As the simulation begins with an initial infection, the simulation must start prior to the first week of detection by a number of weeks equal to the assumed infection to detection delay. Relative model weeks assigned to surveillance events are therefore shifted by the assumed detection delay. In the case of a 4-week detection delay, the first detection in the surveillance data occurs not on week 1 but on model week 5. If the toy model has been specified to be used, a toy data set is created from the full surveillance and density data, consisting of an area of an 8 km radius around the first detected case, for the first 20 weeks of data, and brought into the environment instead.

Weeks that define the winter period (ii)

A vector of which weeks of the year are to be classified as the winter period informs both infectious period estimates and seasonal recovery rates. These weeks were previously defined from weekly averages of local meteorological data as a continuous series of week numbers bound by the earliest and latest week in winter with a mean temperature no greater than 5°C. This vector is converted to relative model weeks across the full simulation time period (e.g. week 1 in the second year is considered to be relative week 53), enabling seasonality across multiple year periods.

Cell infectious periods (iii)

Cell infectious periods, accounting for the assumed detection delay and seasonal differences (winter/non-winter) based on which weeks are classified as winter, are estimated from gridded surveillance data to inform seasonal recovery rates and calculate observed summary statistics. The infectious period of each cell is calculated as the summation of overlapping individual infectious periods for each found dead detected carcass within that cell. To estimate the infectious period of a carcass, both the detection delay duration (defined as the time from

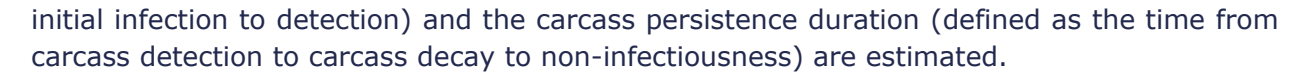
EFSA Supporting publication 2024:EN-9049

www.efsa.europa.eu/publications





led from https://efsa.on/inel/brary.wiley.com/doi/10.2903/sp. efsa. 2024.EN-9049 by Istituto Zooprofilattico Sperimenta ed Il'Umbria e delle Marche (IZSUM), Wiley Online Library on [0.41/2.2024]. See the Terms and Conditions) on Wiley Online Library on rules of use; OA articles are governed by the applicable Ceretive Commons



The detection delay itself is the sum of the time from infection to death and the estimated time it takes for a surveillance team to find a carcass. The former is estimated at two weeks (Guinat et al., 2018). The estimated delay in carcass detection, through expert opinion on levels of carcass decomposition upon discovery in a highly-surveilled setting (South Korea), is also approximately two weeks (J.-S. Lim, personal communication, May 2024). Together this yields an estimated detection delay of four weeks per carcass. As the latent period for ASF in wild boar is only a few days, it was assumed to play a negligible role in infection dynamics at this scale (Blome et al., 2013; Pietschmann et al., 2015). Accordingly, the detection delay becomes synonymous with the pre-detected infectious period.

Carcass persistence and environmental infectiousness is known to be seasonally-dependent, with longer persistence durations observed in colder months (Guberti et al., 2022). Here, wild boar carcass infectiousness is assumed to persist on average for four weeks from death, with the value extended to six weeks from death during winter, based on EFSA expert opinion. In reference to carcass detection, this translates to an environmental infectiousness persistence of two- and four-weeks post-detection for the non-winter and winter periods, respectively.

Having estimated both detection delay and environmental infectiousness persistence durations, the complete infectious periods for all detected positive carcasses can be estimated per cell per week.

(iv) Weekly detection rates

Per-cell weekly detection rates are calculated from the surveillance data. The probability of detection in infectious cell i at week t is seen as a function of the mean prevalence within a cell upon first detection and the total number of carcasses tested that week (Equation A1),

$$P_{i,t} = 1 - (1 - \pi_{det})^{n_{i,t}} \tag{A1}$$

where $P_{i,t}$ is the probabilty of detection in cell i at week t, π_{det} is mean prevalence around first detection in the study area, and $n_{i,t}$ is the number of tested carcasses in cell i at week t. The mean prevalence around first detection is also derived from the surveillance data. Spatiotemporal windows of 2, 4, 6, 8 and 10 km and 2, 4 and 6 weeks around each case that were first detected in each cell are examined, and within each window the proportion of positive carcasses per total number of tested carcasses is calculated (excluding instances of only a single positive case). The mean of these observed prevalences is thereafter used to inform the prevalence parameter. Detection rates are then calculated per cell per week following a log function (Equation A2),

$$\varepsilon_{i,t} = -\ln(1 - P_{i,t}) \tag{A2}$$

where $\varepsilon_{i,t}$ is the detection rate for infectious cell i at week t and $P_{i,t}$ is the probabilty of detection in cell i at week t.

www.efsa.europa.eu/publications







ded from https://efsa.onlinelibrary.wilety.com/doi/10.2903/sjp.efsa.2024.EN-9049 by Istituto Zooprofilattico Sperimenta dell'Umbria e delle Marche (IZSUM), Wiley Online Library on [04/12/2024]. See the Terms and Conditions) on Wiley Conline Library for rules of use; OA articles are governed by the applicable Ceretive Commons



(v) Seasonal recovery rates

Recovery rates for the winter and non-winter seasons are calculated from the estimated infectious period durations for each season.

Epidemic wave-end weeks

The weeks at which an epidemic wave ends are derived from the observed cell-level incidence and used to enable cell transitions from the recovered state back to the susceptible state. These weeks are then converted into model time (i.e. which relative weeks specify wave ends).

(vii) Contact index

The contact index, specifying which cells are in contact, is generated from the density grid data according to the Moore neighbourhood of each cell.

(viii) Initial infected

The initially-infected cells are identified from the surveillance data as all cells that had a positive case in the first ISO week of the data.

(ix) Normalised cell density

In order to estimate the relative effect of density, the absolute density values of all cells are normalised to [0, 1] across the study area.

A.3.4.1.2. Generate priors

In the parameter calibration phase, priors are generated from fixed uniform distributions for the parameters that have been specified to be estimated (Table A.3). In the parameter evaluation phase, the particle set estimated during the calibration phase is used instead.

For generating prior distributions, due to the Latin hypercube sampling method of particle selection used in the APMC parameterisation algorithm, all priors must follow uniform distributions. If a static transmission rate is employed in the simulation, the priors for the transmission rate equal the transmission rate in the simulation. If a seasonal transmission rate is employed, the priors that are generated inform the construction of the sinusoidal function (of a 52-week period), from which weekly transmission rates are calculated. Here, priors are generated for both amplitude (A) and phase shift (υ) of the sine wave. The amplitude prior range is equal to the static transmission rate prior range, while the phase shift range allows the sinusoidal function to peak at any point along its annual cycle. The amplitude and phase shift priors are translated to estimations of the maximum transmission rate (β_{max}) and the week of the year at which the maximum transmission rate occurs ($t_{\beta_{max}}$). Of note, a non-zero minimum baseline transmission rate was also attempted to be included in sinusoidal function estimation, however doing so would force errors in the APMC algorithm (likely due to issues with the covariance matrix producing non-positive eigenvectors during





ded from https://efsa.onlinelibrary.wilety.com/doi/10.2903/sjp.efsa.2024.EN-9049 by Istituto Zooprofilattico Sperimenta dell'Umbria e delle Marche (IZSUM), Wiley Online Library on [04/12/2024]. See the Terms and Conditions) on Wiley Conline Library for rules of use; OA articles are governed by the applicable Ceretive Commons

particle perturbation) and is not possible at this time. If relative susceptibility (ϕ) or relative infectivity (ψ) parameters are employed, priors are generated for each parameter.

Table A.3. Priors

Parameter	Prior	Units	Activation
Transmission rate (β)	~ Uniform(0, 2)	Cells infected per week by a single cell	If sine_beta = FALSE
Amplitude (A)	~ Uniform(0, 2)	Maximum cells infected per week by a single cell	If sine_beta = TRUE
Phase shift (u)	~ Uniform(0, 2)	Radians	If sine_beta = TRUE
Relative susceptibility (ϕ)	~ Uniform(0, 1)	n/a	If rel_sus = TRUE
Relative infectivity (ψ)	~ Uniform(0, 1)	n/a	If rel_inf = TRUE

Compute summary statistics A.3.4.1.3.

Summary statistics reflecting the temporal, spatial, and density components of the observed data are calculated from the cell infectious periods and density grid data. Depending on the duration of the period over which the statistics are to be calculated (specified during initialisation), a vector is produced of cell incidence, the area of the minimum convex polygon around detected cells, and the total wild boar density of infectious-detected cells for each period of specified weeks in the observed data.

A.3.4.1.4. Run epidemic simulation

Following generation of model data structures and parameter prior distributions, the script containing the simulation module is loaded ("scripts/02.2-RunSim.R") and data is simulated via the epidemic simulation module inside the APMC algorithm. Here, particles (sets of parameter values) are sampled from the prior distributions, and the APMC algorithm runs multiple generations of simulations until posterior distributions are determined (see §A.3.4.1.4(vi) for detail).

(i) Draw particles

In the parameter calibration sub-model, initial particles are drawn from the provided prior distributions via Latin hypercube sampling and are used to simulate data.

(ii) Assign cells to initial states

EFSA Supporting publication 2024:EN-9049

www.efsa.europa.eu/publications

The present document has been produced and adopted by the bodies identified above as authors. This task has been carried out exclusively by the authors in the context of a contract between the European Food Safety Authority and the authors, awarded following a tender procedure. The present document is published complying with the transparency principle to which the Authority is subject. It may not be considered as an output adopted by the Authority. The European Food Safety Authority reserves its rights, view and position as regards the issues addressed and the conclusions reached in the present document, without prejudice to the rights of the authors.





on linelibrary wiley com/doi/10.2903/sp. efsa.2024.EN-9049 by Istituto Zooprofilatico Sperimenta dell'Umbria e delle Marche (IZSUM), Wiley Online Library on [04/12/2024]. See the Terms

All cells are assigned to the susceptible state except for those defined as initially infectious, which are assigned to the infectious-undetected state.

Calculate weekly transmission rates

If the simulation uses a static transmission rate, no further transmission rate calculations are performed. Otherwise, if the transmission rate in the simulation is specified to follow a sinusoidal function, the amplitude and phase shift particle values are used to calculate weekly transmission rates across the study period per Equation A3

$$A * (1 + \sin\left(2\pi * \frac{t_{weeks}}{52} + v\right) \tag{A3}$$

where A is the amplitude, t_{weeks} is the week of simulation and v is the phase shift.

(iv) Calculate relative susceptibility and infectivity of cell

The relative susceptibility of a cell is calculated as a function of its normalized density per Equation A4

$$\varphi_j = \rho_j + \varphi(1 - \rho_j) \tag{A4}$$

where φ_i is the relative susceptibility of cell j, ρ_i is the normalized density of cell j, and φ is the estimated relative susceptibility. The relative infectivity of a cell is calculated as a function of its normalized density per Equation A5

$$\psi_i = \rho_i + \psi(1 - \rho_i) \tag{A5}$$

where ψ_i is the relative infectivity of cell i, ρ_i is the normalized density of cell i, and ψ is the estimated relative infectivity.

Epidemic data simulation (v)

The simulation module operates in discrete time step of one-tenth of a week. This follows general guidelines for the τ -leap method of stochastic system approximation, a modification of the Gillespie stochastic system algorithm (Gillespie, 2001; Keeling & Rohani, 2008). At each time step t, the following sequence of events occurs:

- 1. The environment updates global simulation variables for the new time step.
 - a. The infection state matrix is updated with the status of all cells from the previous time step.
 - b. The infectious-undetected state timer statuses are updated for all cells.
 - i. Any units that have been in the infectious-undetected state have their timer advanced by 1.
 - ii. Any units that have left the infectious-undetected state have their timer deactivated (set to -1).

www.efsa.europa.eu/publications







rom https://efsa.onlinelibrary.wikey.com/doi/10.2903/sp.efsa.2024.EN-9049 by Istituto Zooprofilatico Sperimenta dell'Umbria e delle Marche (IZSUM), Wikey Online Library on [04/12/2024]. See the Terms and Conditions (https://onlinelibrary.wiley.com/etms-and-conditions) on Wiley Online Library for rules of use; OA articles are governed by the applicable Cereive Commons



- iii. Any units that have entered the infectious-undetected state during the previous timestep have their infectious-undetected timer started (set to 0).
- c. The week of the model is calculated from the time step.
- 2. The force of infection (λ) on susceptible cells follows a frequency-dependent construction and is calculated for all susceptible cells experiencing non-zero infection pressure from contacts defined in the contact index, per Equation A6

$$\lambda_j = \varphi_j \sum_{t \in I_j} \psi_i * \beta_t / N_i \tag{A6}$$

where λ_j is the force of infection exerted on susceptible cell j, φ_i is the relative susceptibility of cell j, ψ_i is the relative infectivity of infectious cell i, β_t is the transmission rate (at week t if seasonal), and N_i is the number of cells in the Moore neighbourhood of cell i (equal to 8 except for cells on a border), and I_i is the set of all infectious cells around cell j.

- 3. State transitions probabilities are calculated for cells in the susceptible, infectiousundetected, and infectious-detected states. Stochastic transitions between the susceptible, infectious-undetected, infectious-detected, and recovered states follow exponentially-distributed transition rates, informed by the force of infection, detection rate, or recovery rate, respectively. Units in the infectious-undetected state are only able to transition once they have been in that state for at least two weeks, aligned with the minimum estimated time it takes from initial infection to production of a carcass in a cell. Cells in the recovered state transition back to the susceptible state if they are in the recovered state during the week of the year specified to signal the end of an epidemic wave.
- 4. The infection state matrix is updated with the new infection states for all units at time t, and the loop restarts at the next time step t+1 until all time steps are exhausted.
- 5. After the simulation has completed its run for all time steps, summary statistics are calculated for the simulation data with the same function used on the observed data in §0. A vector of cell incidence, the area of the minimum convex polygon around detected cells, and the total wild boar density of infectious-detected cells per time period is returned for the APMC algorithm.

(vi) Sub-model termination

The parameter calibration sub-model terminates upon reaching a specified stopping criteria for particle retention. To understand how this criterion is reached, an understanding of the APMC process is required. Though a full description of ABC-SMC processes is beyond the scope of this report, a short summarisation of the APMC methodology follows.





397832,5. 2024. 11, Downloaded from https://esta.onlinelbrary.vitey.com/doi/10.2903/sp.cfsa.2024.EN-9049 by Istituto Zoprofollatics Sperimenta dell'Umbria e delle Marche (IZSUM), Wiley Online Library on [04172024]. See the Terms and Conditions, universal conditions on Wiley Online Library on Public Online Library on Public Online Common Library on [04172024]. See the Terms and Conditions on Wiley Online Library on Wiley Online Library on Public Online Common Library on [04172024]. See the Terms and Conditions on Wiley Online Library on Wiley Online Library on [04172024]. See the Terms and Conditions on Wiley Online Library on [04172024]. See the Terms and Conditions on Wiley Online Library on [04172024]. See the Terms and Conditions on Wiley Online Library on [04172024]. See the Terms and Conditions on Wiley Online Library on [04172024]. See the Terms and Conditions on Wiley Online Library on [04172024]. See the Terms and Conditions on Wiley Online Library on [04172024]. See the Terms and Conditions on Wiley Online Library on [04172024]. See the Terms and Conditions on Wiley Online Library on [04172024]. See the Terms and Conditions on Wiley Online Library on [04172024]. See the Terms and Conditions on Wiley Online Library on [04172024]. See the Terms and Conditions on Wiley Online Library on [04172024]. See the Terms and Conditions on [04172024]. See the Terms an



In ABC-SMC methods, a set of particles is sampled from the prior distributions, of length equal to the number of simulations specified during model initialisation. Data is simulated (by the epidemic simulation module) for each particle, and the distance between the simulated and observed data is calculated (the distance being measured via summary statistics). As summary statistics almost invariably involve different scales or units, the summary statistics are normalized by equalizing their variance. This results in equal weighting across all summary statistics, and prevents summary statistics with large variances from governing the comparison to the observed data. The simulated and observed data is compared, and the distance is defined by the maximum absolute distance value among all summary statistics. A previously computed tolerance value that determines the maximum allowable distance between the simulated and observed data for a particle to be accepted is applied to the distances for each particle. Particles that had produced simulated data within the tolerance level to the observed data are then accepted, and a particle acceptance rate is computed. Weights are applied to the retained particles based on their closeness to the observed data, and new particles are generated to replace those that were not accepted. To augment exploration of the parameter space, particles are slightly perturbed. The process repeats with new data being simulated from the updated particle set. In the next generation of simulation, a lower (stricter) tolerance level is computed, decreasing the number of accepted particles and forcing accepted particles to simulate data closer to the observed data. As the tolerance level decreases, the particle acceptance rate falls. The APMC algorithm stops once the particle acceptance rate falls below the minimum acceptance rate (set by default to 0.05), as only minimal improvement in the convergence of the posterior distribution would be seen should the calibration process continue. Upon termination, a data object including conserved particles and the final distance to the observed data for the model is returned. The results of 500 simulations are examined at each calibration step, with a default particle rejection proportion of 0.5 (yielding 250 conserved particles after each step).

A.3.4.2. Particle testing sub-model

The particle set generated from the calibration sub-model is now used to simulate data for each particle. Each particle is fed into the simulation and a summary of infection state transitions for all cells is returned for each simulation. After all particles are ran and results returned, the summary tables are catenated into a list and attached to the object containing the model calibration metrics. This object is then saved as "data/gen/results_model_#.rds", where # indicates the model identification number (1-8) provided during job submission.

A.3.5. **Analysis**

Upon job completion, eight models (each employing a different parameter combination) will have been ran, and the output data will have been generated for each model. This data can be imported locally (following the same directory structure), and analysed via the script "scripts/03-analysis.R". Here, the final distances between the summary statistics for the simulated and observed data are compared, and the best fitting model is defined as the one with the smallest distance. The best-performing model is used to examine posterior distributions for conserved parameters, seasonal transmission rate (if necessary, depending on the model), both apparent and true simulated incidence, detection probabilities per cell,

www.efsa.europa.eu/publications







3978325, 2024, 11, Downloaded from https://efsa.onlinelibrary.wiley.com/doi/10.2903/sp.efsa.2024.EN-9049 by Istituto Zooprofilatico Sperimenta dell'Umbria e delle Marche (IZSUM), Wiley Online Library on [04/12/2024]. See the Terms

and-conditions) on Wiley Online Library for rules of use; OA articles are governed by the applicable Creative Commons



and discrimination ability through a receiver operating characteristic (ROC) curve. Density is concluded as playing an influential role in explaining the observed epidemic dynamics if the best-performing model includes at least one parameter informed by wild boar density (i.e. relative susceptibility, relative infectivity, or both). To determine if the impact of wild boar density is specific to individual epidemic waves, the null model that shared the same transmission rate function as the best performing model—the model that was parameterised by only a transmission rate without any influence of wild boar density—is used to provide the scenario under which density would have no effect on transmission. Proportions of detected cells that are above the median density of the study area for the observed data are compared to the 95% prediction intervals from the simulated data of null scenario, and if the observed proportion is above the null simulation prediction interval, it can be concluded that density was a factor in shaping transmission in that wave.

A.3.6. **Implementation**

The ASF wild boar density assessment model was constructed and implemented in R, version 4.4.1 "Race for Your Life" (R Core Team, 2024). All levels of implementation utilized features and functions from the Tidyverse suite of packages (Wickham et al., 2019). Spatial statistics and spatial analysis were performed through the Simple Features package (Pebesma, 2018). Parameter calibration was performed through the EasyABC package (Jabot et al., 2023). All cartographic plots were generated via the tmap package (Tennekes, 2018).